Available online at www.sciencedirect.com
ScienceDirect
Continental Shelf Research 26 (2006) 1571–1594
CONTINENTAL SHELF RESEARCH
www.elsevier.com/locate/csr

Development and application of a three-dimensional orthogonal coordinate semi-implicit hydrodynamic model

S. Sankaranarayanan*, Matthew C. Ward

Applied Science Associates, 70, Dean Knauss Drive, Narragansett, RI-02882, USA

Received 19 May 2005; received in revised form 31 March 2006; accepted 14 April 2006
Available online 30 June 2006

Abstract

A three-dimensional, orthogonal coordinate semi-implicit hydrodynamic model in spherical coordinates that can be applied to estuarine, coastal sea, and continental shelf waters is presented. A generalized orthogonal coordinate transformation on the horizontal and a sigma coordinate transformation on the vertical, are applied to the governing equations. The governing equations are decomposed into exterior and interior modes and solved using a semi-implicit solution technique. Second-order accurate spatial and temporal discretization schemes are used on a space staggered grid. A simple flooding and drying technique is used to model the tidal flats. The model results are tested against analytical solutions for tidal circulation in an annular channel and steady residual flow generated by wind, and density differences in a rectangular channel. The predictions from the model showed very good comparison with analytical solutions for all the test cases. Three-dimensional circulation in Narragansett Bay was then studied using the developed model. The model predicted surface elevations, three-dimensional instantaneous and mean currents, salinities, and temperatures in Narragansett Bay are compared with the observations. Mean errors in the model predicted surface elevations and velocities are less than 3% and 15%, respectively. The spring and neap cycles, the shorter duration but stronger ebb dominant currents and the double flood phenomena seen in the observations are reproduced by the model. The mean estuarine currents, and the sub-tidal currents seen in the observations are also well reproduced by the model. Correlation coefficients for salinity and temperatures exceed 0.95 and 0.87, respectively.

Keywords: Orthogonal; Semi-implicit; Hydrodynamic model; Narragansett Bay

1. Introduction

Three-dimensional hydrodynamic models using different numerical techniques have been used to predict circulation and transport in estuarine, coastal and shelf waters. Some of the early hydrodynamic models employed finite difference schemes on square grids. Boundary-fitted models (Spaulding, 1984; Sheng, 1986; Swanson, 1986; Muin and Spaulding, 1997a) using non-orthogonal grids have the flexibility to generate grids for domains with complex geometries. The transformation of the shallow water equations in a boundary-fitted coordinate system generates several extra terms in the momentum equations (Muin and

*Corresponding author. Tel.: +1 401 7828863; fax: +1 401 7891932.
E-mail addresses: sankar@appsci.com (S. Sankaranarayanan), wardm@appsci.com (M.C. Ward).

0278-4343/$ - see front matter © 2006 Elsevier Ltd. All rights reserved.
doi:10.1016/j.csr.2006.04.004

Spaulding, 1996). Sankaranarayanan and Spaulding (2003a) showed through analytical model testing and truncation error analysis that the error in the model predictions increases as the grid angles deviate from orthogonality in a Boundary-fitted coordinate system. On the other hand, orthogonal curvilinear coordinate transformations (Blumberg and Herring, 1987; Hamrick, 1995; Willemse et al., 1985; Song and Haidvogel, 1994) generates only a fewer extra terms, but retaining the simplicity of the familiar Cartesian coordinate equations.

The Estuarine Coastal Ocean model (ECOM) developed by Blumberg and Mellor (1987) uses explicit external mode and implicit internal mode solutions, with the external mode requiring smaller time steps. The Environmental Fluid Dynamics Code (EFDC) developed by Hamrick (1995) is another orthogonal curvilinear coordinate hydrodynamic model that uses semi-implicit external mode and implicit internal mode solutions. The present model uses the governing equations in a spherical coordinate system and hence can be applied to large geographical regions, whereas ECOM and EFDC use equations in a Cartesian coordinate system.

It should also be noted that it could be rather difficult to generate orthogonal grids, fitting complex coastlines, without deviating from grid orthogonality. Attempts to generate exact orthogonal grids for complex coastlines with internal island groups using elliptical grid generation techniques met with limited success (Chan et al., 1994). Eca (1996) was able to generate nearly orthogonal grids with the use of control functions, and by a judicious movement of boundary points.

Finite Element Methods (FEMs) also have the capability to represent complex geometries in a natural way, using triangular and quadrilateral elements. Early applications of FEM to shallow water equations using Galerkin methods exhibited extreme oscillations in the solution that had to be damped with large amounts of viscosity. Lynch and Gray (1979) found that the transformation of the continuity equation to a higher-order wave equation eliminated the oscillations seen in earlier FEM solutions. Ip et al. (1998) developed a finite element model using a two-dimensional kinematic form of the wave equations, including a Darcian flow component for simulating flow during wetting and drying. Walters (2005) gives a good historical view of the developments in FEM for solving shallow water equations. Stelling and Duinmeijer (2003) have proposed a numerical technique with staggered grids, using numerical integration techniques, that can be applied to rapidly varied flow problems such as hydraulic jumps and bores and large scale inundation problems.

Recently, Finite Volume Methods (FVM) that combine the advantages of finite element (for geometric flexibility) and finite difference methods (for ease of calculation of fluxes through faces) have been used to solve shallow water equations. (Ward, 1999; Chen et al., 2003; Zhang et al., 2004).

The sigma coordinate system used in the vertical direction uses the same number of layers, independent of its depth and hence it is very effective in resolving shallow regions. Estuaries with no abrupt changes in bathymetry are modeled well using sigma coordinate system (Oey et al., 1985). However, the sigma coordinate system is known to introduce errors in the baroclinic pressure gradient terms, while encountering sharp topographic changes such as shelf breaks and has been discussed in detail in the literature (Mellor et al., 1994; Haney, 1991). Mellor et al. (1998) classified the errors due to sigma coordinate pressure gradient as two types namely, (i) sigma error of the first type caused due to two-dimensional baroclinic terms, that decays with time and hence rather benign, and (ii) sigma error of the second type that occurs in three-dimensional flows. Many numerical schemes have been proposed to reduce the errors due to sigma coordinate system (Stelling and van Kester, 1994; Slordal, 1997; Chu and Fan, 1997; Shchepetkin and McWilliams, 2003; Huang and Spaulding, 1996, 2002). Luo et al. (2002) developed an eta-coordinate version of the Princeton Ocean Model and showed the reduction in pressure gradient errors over sigma coordinate systems for the seamount problem with steep slopes. Sigma coordinate systems are continuous at the surface and bottom, whereas eta-coordinate system is continuous at the surface and stepwise at the bottom. Eta-coordinate system developed by Messinger (1984) is currently used in many numerical atmospheric models (http://meted.comet.ucar.edu/nwp/pcu2/index.htm).

The main objective of this paper is to present the development, testing and application of a three-dimensional hydrodynamic model with generalized orthogonal curvilinear coordinates on the horizontal and a sigma coordinate on the vertical, that can be rapidly implemented for real-time forecasting in coastal and estuarine waters. Some of the recent developments in hydrodynamic modeling outlined

in this study show a lot of promise for solving situation specific problems, such as rapidly varied flows (Stelling and Duinmeijer, 2003), but their use in real-time forecasting of a generic water body may not be warranted. The model reported in this study retains the semi-implicit time integration techniques given in Muin and Spaulding (1997a). Since the governing equations in the present study are very different than that given in Muin and Spaulding (1997a), the model results are tested against analytical solutions for tidal circulation in an annular channel. The model was also tested against steady residual flow generated by wind and density differences in a rectangular channel. The model is then applied to study the three-dimensional circulation in Narragansett Bay. Skill assessment of the model is performed, by comparing the model predictions with the observations in Narragansett Bay.

2. Governing equations

The equations of motion and continuity are expressed in a generalized orthogonal curvilinear coordinate system (Kantha and Clayson, 2000) on the horizontal, with the ability to resolve arbitrary topography and also the flexibility to refine the grid in regions of particular interest. The derivation of metric tensors (scale factors) in a spherical coordinate system is given in Appendix B. An independent sigma coordinate system is applied on the vertical to resolve bathymetric variations with a constant number of layers.

2.1. Continuity equation:

$$R\sqrt{g_{11}g_{22}}\frac{\partial\zeta}{\partial t}+\frac{\partial\left(uD\sqrt{g_{22}}\right)}{\partial\xi}+\frac{\partial\left(vD\sqrt{g_{11}}\right)}{\partial\eta}+R\sqrt{g_{11}g_{22}}\frac{\partial\omega}{\partial\sigma}=0. \tag{1}$$

Momentum equation in ξ-direction:

$$\frac{\partial uD}{\partial t}+\frac{1}{R\sqrt{g_{11}g_{22}}}\left[\frac{\partial\left(u^2D\sqrt{g_{22}}\right)}{\partial\xi}+\frac{\partial\left(uvD\sqrt{g_{11}}\right)}{\partial\eta}+uvD\frac{\partial\left(\sqrt{g_{11}}\right)}{\partial\eta}-v^2\frac{\partial\left(\sqrt{g_{22}}\right)}{\partial\xi}\right]$$
$$+\frac{\partial u\omega}{\partial\sigma}-fDv=-\frac{gD}{R\sqrt{g_{11}}}\left[\frac{\partial\zeta}{\partial\xi}+\frac{D}{\rho_0}\int_\sigma^0\left(\frac{\partial\rho}{\partial\xi}-\frac{\sigma}{D}\frac{\partial D}{\partial\xi}\frac{\partial\rho}{\partial\sigma}\right)\mathrm{d}\sigma\right]+\frac{1}{D}\frac{\partial}{\partial\sigma}\left(A_v\frac{\partial u}{\partial\sigma}\right). \tag{2}$$

Momentum equation in η-direction:

$$\frac{\partial vD}{\partial t}+\frac{1}{R\sqrt{g_{11}g_{22}}}\left[\frac{\partial\left(uvD\sqrt{g_{22}}\right)}{\partial\xi}+\frac{\partial\left(v^2D\sqrt{g_{11}}\right)}{\partial\eta}+uvD\frac{\partial\left(\sqrt{g_{22}}\right)}{\partial\xi}-u^2\frac{\partial\left(\sqrt{g_{11}}\right)}{\partial\eta}\right]$$
$$+\frac{\partial v\omega}{\partial\sigma}+fDu=-\frac{gD}{R\sqrt{g_{22}}}\left[\frac{\partial\zeta}{\partial\eta}+\frac{D}{\rho_0}\int_\sigma^0\left(\frac{\partial\rho}{\partial\eta}-\frac{\sigma\partial D\partial\rho}{D\partial\eta\,\partial\sigma}\right)\mathrm{d}\sigma\right]+\frac{1}{D\partial\sigma}\left(A_v\frac{\partial v}{\partial\sigma}\right). \tag{3}$$

Conservation of substance:

$$\frac{\partial q}{\partial t}+\frac{1}{R\sqrt{g_{11}g_{22}}}\left[\frac{\partial\left(uq\sqrt{g_{22}}\right)}{\partial\xi}+\frac{\partial vq\sqrt{g_{11}}}{\partial\eta}\right]+w\frac{\partial q}{\partial\sigma}$$
$$=\frac{1}{R^2\sqrt{g_{11}g_{22}}}\left[\frac{\partial}{\partial\xi}\left(\frac{\sqrt{g_{22}}}{\sqrt{g_{11}}}D_h\frac{\partial q}{\partial\xi}\right)+\frac{\partial}{\partial\eta}\left(\frac{\sqrt{g_{11}}}{\sqrt{g_{22}}}D_h\frac{\partial q}{\partial\eta}\right)\right]+\frac{1}{D^2}\frac{\partial}{\partial\sigma}\left(D_v\frac{\partial q}{\partial\sigma}\right), \tag{4}$$

where t is the time, u,v and w the velocities in the ξ, η, and r directions, respectively; f the coriolis parameter; ζ the surface elevation; R the radius of the earth; g the gravity; ρ_0 the average water density; ρ the water density; A_v the vertical eddy viscosity of momentum; D_v the vertical eddy diffusivity of constituent, S the Salinity (psu), Θ the temperature (°C), D_h the horizontal eddy diffusivity of constituent and q is the concentration of a conservative substance such as S or Θ.

Eqs. (1)–(4) assume the following: the flow is incompressible, density differences are neglected unless multiplied by gravity (Boussinesq approximation), the vertical acceleration is small and the horizontal stresses are neglected. The salinity and temperature are related to density through the equation of state (UNESCO, 1981).

Substitutions, $\sqrt{g_{11}}=\sqrt{g_{22}}$ reduces Eqs. (1–4) to that for a conformal coordinate system (Wanstarth, 1977; Lin and Chandler-Wilde, 1996) which is a special case of an orthogonal coordinate system.

Equations for the Cartesian coordinate system can be derived from Eqs. (1)–(4) by substituting, $\sqrt{g_{11}} = \sqrt{g_{22}} = 1$, and $R = 1$.

The parametrization of the sub-grid scale diffusion of turbulence in the vertical direction using turbulent schemes ranging from simple flow-dependent eddy viscosity models (Aldridge and Davies, 1993), and one equation turbulent kinetic energy models (Davies and Jones, 1990; Muin and Spaulding, 1997a) with the length scale specified using the approach suggested by Blackadar (1962) to two-equation turbulence closure models using an equation each for turbulent kinetic energy and mixing length (Blumberg and Mellor, 1987; Blumberg et al., 1992) are now being routinely used in three-dimensional hydrodynamic models. Xing and Davies (1996) showed that there are no significant differences between the tidal currents obtained using a simple eddy viscosity model and that using various turbulence closure models.

In the present study, the sub-grid scale diffusion of turbulence has been parametrized using a simple flow-related eddy viscosity coefficient (A_v). Keeping the eddy viscosity to be vertically constant, the horizontal and temporal variations of A_v were accounted for using the formulation given by Aldridge and Davies (1993) as $A_v(x, y, t) = K * (U^2 + V^2) * D$, where U and V are the vertically averaged velocities in the x and y directions, respectively, and D is the total water depth. The value of K is constant at 0.001. The vertical variations in eddy viscosity and eddy diffusivity, that can be very useful for strongly stratified flows, can be obtained by using a function that depends on gradient Richardson number (Ri) which relates the local gravitational force to the inertial force, suggested by Munk and Anderson (1948) as

$$A_v(z) = A_v(1 + \alpha\, Ri)^{-n}, \tag{5a}$$

$$D_v(z) = D_v(1 + \beta\, Ri)^{-m}, \tag{5b}$$

where $Ri = \dfrac{2g}{\rho h}\dfrac{\partial\rho/\partial\sigma}{(\partial u/\partial\sigma)^2 + (\partial v/\partial\sigma)^2}$ A number of authors have suggested values for the coefficients α, β, m, and n in the above equations (Blumberg, 1986) of which the values ($\alpha = \beta = n = 1$, and $m = 2$) suggested by Officer (1976) is most commonly used. Constants A_v, and D_v can be determined from the mixing length theory or arbitrarily calibrated to the available data.

3. Boundary conditions

The surface and bottom boundary conditions are given by

$$\text{At the surface } \sigma = 0,\ \frac{A_v}{D}\left(\frac{\partial u}{\partial\sigma}, \frac{\partial v}{\partial\sigma}\right) = C_a\rho_a\left(\sqrt{W_\xi^2 + W_\eta^2}\right)\ (W_\xi,\ W_\eta). \tag{6}$$

$$\text{At the bottom } \sigma = -1, \frac{A_v}{D}\left(\frac{\partial u}{\partial\sigma}, \frac{\partial v}{\partial\sigma}\right) = C_d\rho_0(\sqrt{u^2 + v^2})\ (u, v), \tag{7}$$

where ρ_a is the density of air; ρ_0 the density of water; W_ξ and W_η the wind speeds, respectively in the ξ and η directions, respectively ; and C_a and C_d is the quadratic surface and bottom drag coefficients.

The vertical boundary conditions are

$$w = 0 \text{ at } \sigma = 0 \text{ and } \sigma = -1. \tag{8}$$

The land boundaries are assumed impermeable, the normal component of the velocity is set to zero. Sea surface elevation or tidal harmonic constituents can be specified as a function of time along the open boundaries, as a classic Dirichlet condition. Alternatively, a Sommerfield radiation boundary condition (Sommerfield, 1979) can be used as

$$\frac{\partial\zeta}{\partial t} + \frac{c}{R\sqrt{g_{11}}}\frac{\partial\zeta}{\partial\xi} = 0 \quad \text{and} \quad \frac{\partial\zeta}{\partial t} + \frac{c}{R\sqrt{g_{22}}}\frac{\partial\zeta}{\partial\eta} = 0, \tag{9}$$

which allows the wave propagating towards an eastern boundary exit undisturbed through that boundary.

At the closed boundaries the transport of substance is zero. At the open boundaries, the concentration should be specified during the inflow. On outflow, the substance is advected out of the model domain according to

$$\frac{\partial q}{\partial t} + \frac{u}{R\sqrt{g_{11}}}\frac{\partial q}{\partial\xi} \quad \text{and} \quad \frac{\partial q}{\partial t} + \frac{v}{R\sqrt{g_{22}}}\frac{\partial q}{\partial\eta} = 0. \tag{10}$$

Net heat flux is applied at the surface, while solving the thermal transport equation. Net heat flux is given by

$$\text{Net heat flux } (\mathrm{W/m^2}) = H_s - H_l - H_c - H_e,$$

where H_s is the solar radiation, which can be obtained from National Climatic Data Center, H_c the conductive heat flux that occurs between the atmosphere and water body, based on Edinger et al. (1974), H_l the net atmospheric radiation as a result

of downward radiation from the atmosphere and the upward radiation emitted by the water surface and H_e is the evaporative heat flux, related to the conductive heat flux through Bowens ratio, based on Edinger et al. (1974).

A recent application of Edinger's formulations to simulate water column heating in Onondaga lake can be found in Ahsan and Blumberg (1999).

4. Two-dimensional vertically averaged equations of motion and continuity

The three-dimensional hydrodynamic equations (Eqs. (1)–(3)), contain fast moving external gravity waves and slow moving internal gravity waves. The equations of motion are split into vertically averaged equations (exterior mode) and vertical structure equation (interior mode). This technique allows the calculation of free surface elevation from the exterior mode and the three-dimensional currents and thermodynamic properties from the interior mode. The external mode equations are obtained by integrating Eqs. (1)–(3) from $\sigma = 0$ to -1.

The vertically averaged continuity equation is given by

$$R\sqrt{g_{11}g_{22}}\frac{\partial \zeta}{\partial t} + \frac{\partial (UD\sqrt{g_{22}})}{\partial \xi} + \frac{\partial (VD\sqrt{g_{11}})}{\partial \eta} = 0. \quad (11)$$

Momentum equation in ξ-direction:

$$\frac{\partial UD}{\partial t} + \frac{1}{R\sqrt{g_{11}g_{22}}}\left[\frac{\partial \left(U^2 D\sqrt{g_{22}}\right)}{\partial \xi} + \frac{\partial \left(UVD\sqrt{g_{11}}\right)}{\partial \eta} + UVD\frac{\partial \left(\sqrt{g_{11}}\right)}{\partial \eta} - V^2\frac{\partial \left(\sqrt{g_{22}}\right)}{\partial \xi}\right]$$
$$- fDV = -\frac{gD}{R\sqrt{g_{11}}}\left[\frac{\partial \zeta}{\partial \xi} + \frac{D}{\rho_0}\int_{-1}^{0}\int_{\sigma}^{0}\left(\frac{\partial \rho}{\partial \xi} - \frac{\sigma}{D}\frac{\partial D}{\partial \xi}\frac{\partial \rho}{\partial \sigma}\right)\mathrm{d}\sigma\right]. \quad (12)$$

Momentum equation in η-direction:

$$\frac{\partial VD}{\partial t} + \frac{1}{R\sqrt{g_{11}g_{22}}}\left[\frac{\partial \left(UVD\sqrt{g_{22}}\right)}{\partial \xi} + \frac{\partial \left(V^2 D\sqrt{g_{11}}\right)}{\partial \eta} + UVD\frac{\partial \left(\sqrt{g_{22}}\right)}{\partial \xi} - U^2\frac{\partial \left(\sqrt{g_{11}}\right)}{\partial \eta}\right]$$
$$+ fDV = -\frac{gD}{R\sqrt{g_{22}}}\left[\frac{\partial \zeta}{\partial \eta} + \frac{D}{\rho_0}\int_{-1}^{0}\int_{\sigma}^{0}\left(\frac{\partial \rho}{\partial \eta} - \frac{\sigma}{D}\frac{\partial D}{\partial \eta}\frac{\partial \rho}{\partial \sigma}\right)\mathrm{d}\sigma\right]. \quad (13)$$

5. Solution methodology

The two-dimensional vertically averaged equations of motion and continuity are solved using a semi-implicit method (Madala and Piacsek, 1977; Swanson, 1986; Muin and Spaulding, 1996; Ward, 1999) in which the surface elevation is solved implicitly while the other terms in the equation such as the Coriolis, bottom stress, density gradient, and advective terms are solved explicitly. The momentum equations are substituted into the continuity equation to obtain a Helmholtz equation in terms of surface elevation. The spatial discretization is based on a space staggered grid system (Grid C, Arakawa and Lamb, 1977). The velocities u and v are defined at the center of the layer in the vertical direction, but defined at a staggered fashion on the horizontal. The vertical velocity, ω is also defined at the center of the layer in the vertical direction and center of the cell in the horizontal direction. The variables salt, temperature, density, eddy viscosity and eddy diffusivity are also defined at the center of the cell as well. Time is discretized using a three level scheme with a weighting factor of 1.5 (Kinnmark, 1985). Thus the numerical discretization scheme used is second-order accurate in space and time. The discretized Helmholtz equation is solved using sparse matrix method to obtain the surface elevation. The vertically averaged velocities are then obtained from the vertically averaged momentum equations, using the new surface elevation. The stability and dispersion analyses of two-dimensional shallow water equations in curvilinear coordinates for the spatial and temporal discretizations adopted in this study can be found in Sankaranarayanan and Spaulding (2003b). The Shapiro filter (Shapiro, 1970) can be employed as a replacement for simulating sub-grid scale viscosity. The Shapiro

filter helps to eliminate high wave number content in the model fields (Haidvogel and Beckmann, 2000).

The three-dimensional velocities are expressed in terms of the vertically averaged velocity (U,V) and a deviation velocity (u',v') from the vertically averaged velocity. Subtracting the vertically averaged momentum equations from the three-dimensional momentum equations gives the deviation velocity equations of motion:

$$\frac{\partial u' D}{\partial t} = \frac{1}{D}\frac{\partial}{\partial \sigma}\left(A_v \frac{\partial u'}{\partial \sigma}\right) + A, \tag{14}$$

$$\frac{\partial v' D}{\partial t} = \frac{1}{D}\frac{\partial}{\partial \sigma}\left(A_v \frac{\partial v'}{\partial \sigma}\right) + B, \tag{15}$$

where A and B are the non-barotropic terms in the equations of motion and these terms are solved explicitly. The diffusion term is solved implicitly using a three-level scheme to damp out spurious oscillations (Fletcher, 1988). The algorithm is second-order accurate in space and time. A tridiagonal set of equations in the unknown velocity deviation is solved using the Thomas algorithm. The three-dimensional velocity structure is then obtained by adding the vertical deviations of the velocity to the vertically averaged velocities. Both the exterior and interior modes are solved separately. Such a technique has proven to be efficient in solving three-dimensional shallow water equations (Madala and Piacsek, 1977; Swanson, 1986; Muin and Spaulding, 1997a).

The salt and temperature transport equations are solved by a simple explicit technique, except for the vertical diffusion term that is solved by an implicit scheme to ease the time step restriction due to the small vertical length scale. Advection term is solved using an upwind scheme (first-order accurate) that introduces artificial diffusivity. Higher-order upwind schemes (Smolarkiewicz, 1984; Smolarkiewicz and Grobowski, 1990), commonly referred to as Multidimensional Positive Definite Advective Transport Algorithm (MPDATA) have been found

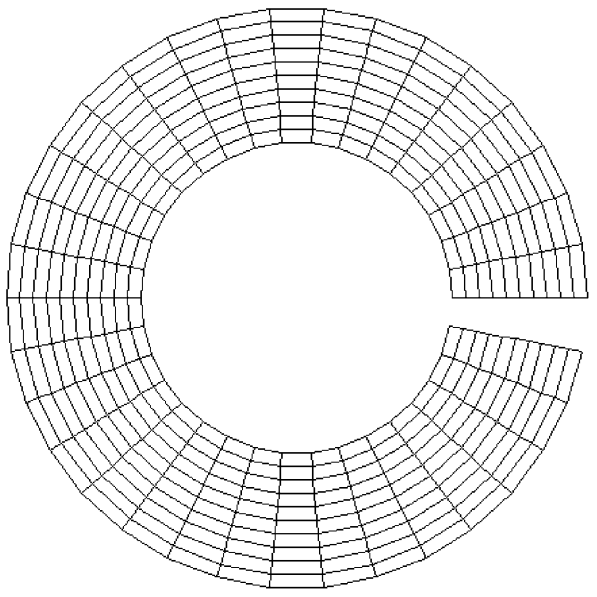

Fig. 1. Grid configuration for Annular Channel Test using a 10×35 grid, with $\Delta r = 3760$ m and $\Delta\theta = 10^\circ$.

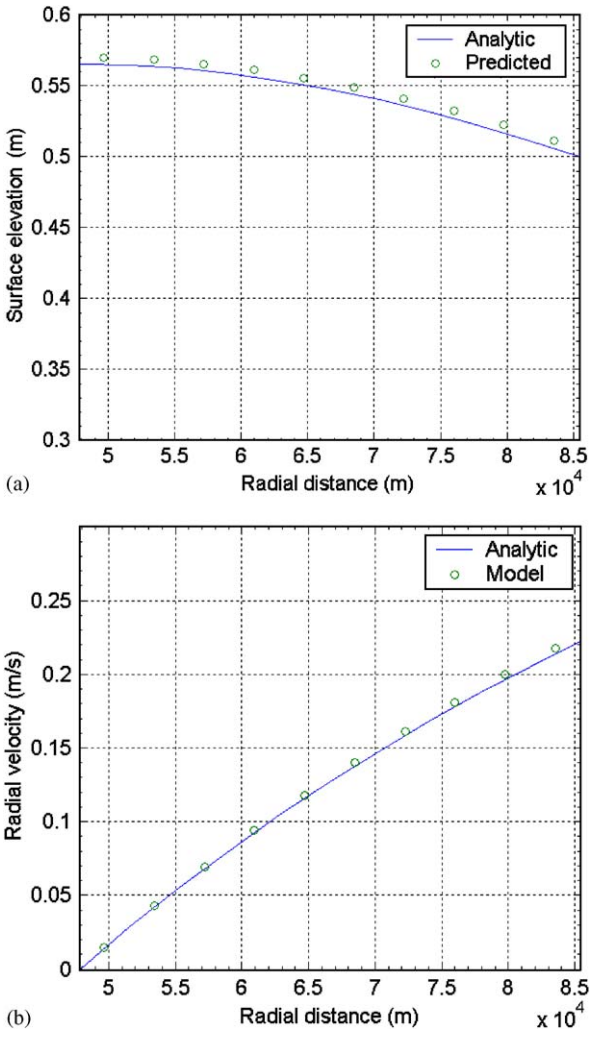

Fig. 2. (a) Comparison of model predictions with analytical solution for surface elevations at maximum forcing amplitude ($\zeta_0 = 0.5$ m, $r_1 = 47{,}800$ m, $r_2 = 85{,}400$ m, $h = 10$ m). (b) Comparison of model predictions with analytical solution for radial velocities at maximum forcing amplitude ($\zeta_0 = 0.5$ m, $r_1 = 47{,}800$ m, $r_2 = 85{,}400$ m, $h = 10$ m).

to be effective in reducing the artificial diffusion introduced by the first-order upwind scheme. A truncated version of the MPDATA, including only the diagonal terms in the diffusion tensor, neglecting the off-diagonal cross derivative terms, has been implemented in the present model, to minimize the artificial diffusion due to the first-order upwind scheme.

5.1. Procedure for wetting and drying

The wetting and drying procedure used in the model presented in this study closely follows the technique outlined in Falconer and Chen (1991). The total water depth (surface elevation + water depth) at the center of the cell is calculated at the end of every time step. If the total depth at any cell is less than the drying height (EDRY), then that cell is allowed to become dry. Then the total water depth at all the four cell faces are calculated and if all the four cell face depths are less than EDRY, then that cell is allowed to become dry. As a grid cell was allowed to dry it was assumed that a thin layer of water remained over the cell. Then as the simulation proceeds, all the dry cells are considered for flooding. If any one of the four surrounding cells are wet, then the water depth at the sides of the cell are calculated and if the water depth is greater than the wetting height (EWET), then that cell is allowed to become wet. In the present model, the values of EDRY and EWET have been kept, respectively, as 0.2 and 0.4 m. Numerical experiments with low values of EDRY and EWET caused numerical instabilities in the solution surface elevations. It should be noted that this flooding and drying procedure could propagate only one grid cell, every time step. Hence, the time step used in the calculations should be less than $\Delta x/\sqrt{gh}$ to minimize the wave-type disturbances at the moving boundary, when the wetting and drying procedure is switched on in the model.

6. Model testing

The model was tested against analytical solutions for tidal circulation in an annular channel, and steady residual flow generated by wind, and density differences in a rectangular channel.

6.1. Tidal forcing in an annular channel

The propagation of a tidal wave into an annular section (350° arc) was performed. At the inner radius and side walls no flow was allowed while the free surface elevation was prescribed to vary sinusoidally in time with uniform amplitude and phase along the outer radius. Neglecting Coriolis and momentum advection terms, the analytical solutions for surface elevation and radial velocity are given by Lynch and Gray (1978) as

$$\zeta(r,t) = Re\{[AJ_0(\beta r) + BY_0(\beta r)]\, e^{i\omega t}\}, \tag{16}$$

$$V_r(r,t) = Re\left\{[-AJ_1(\beta r) - BY_1(\beta r)]\frac{i\omega}{\beta h_0} e^{i\omega t}\right\}, \tag{17}$$

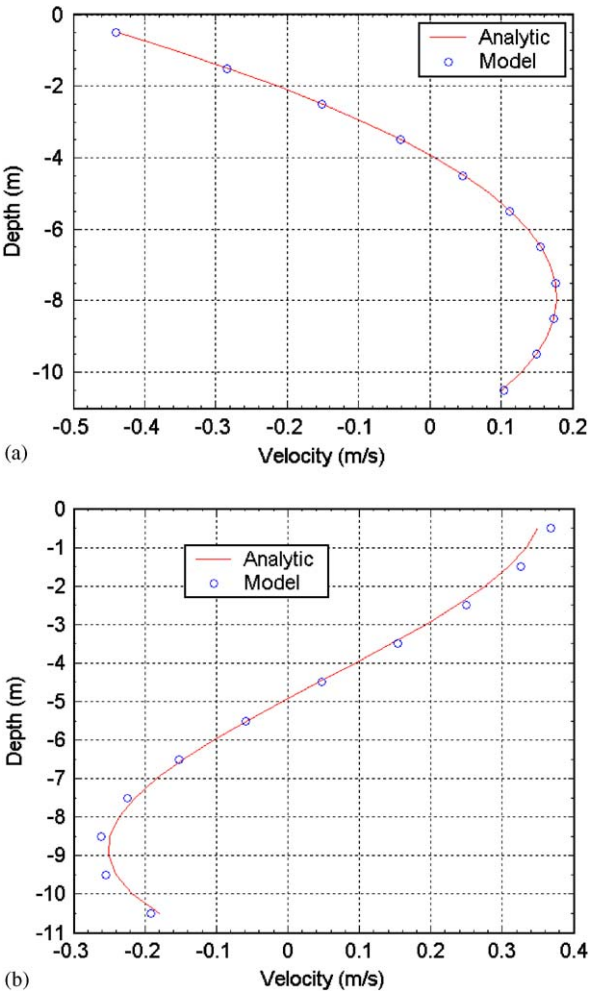

Fig. 3. (a) Comparison of model predicted vertical structure of the longitudinal velocities with analytical solution for wind forcing ($\tau_s = 0.18\,N/m^2$, $A_v = 0.001\,m^2/2$, $k = 0.001$ m/s, $h = 11$ m). (b) Comparison of model predicted vertical structure of the longitudinal velocities with analytical solution for density gradient forcing ($\lambda = 0.001087\,kg/m^4$, $A_v = 0.001\,m^2/s$, $k = 0.001$ m/s, $h = 11$ m).

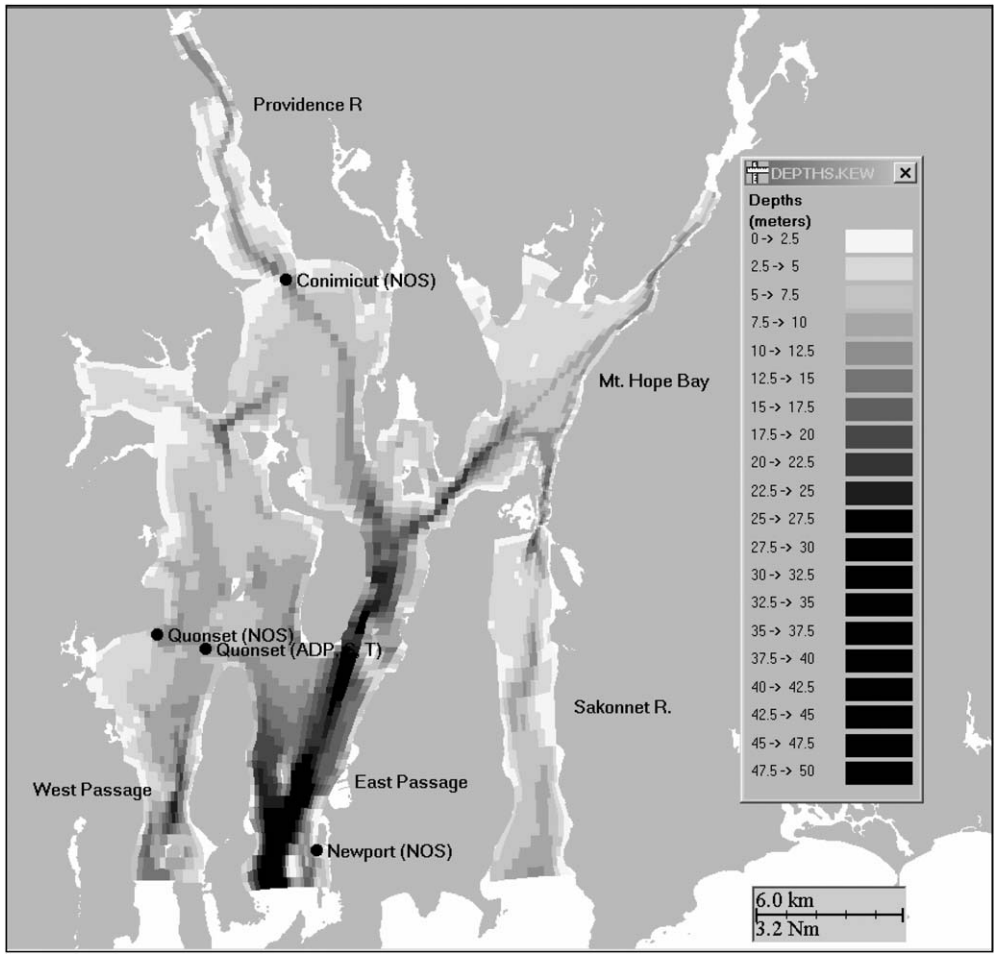

Fig. 4. Narragansett Bay study area and its bathymetry.

where, $A = \zeta_0 Y_1(\beta r_1)/[J_0(\beta r_2 Y_1(\beta r_1) - J_1(\beta r_1))Y_0(\beta r_2)]$, $B = -\zeta_0 J_1(\beta r_1)/[J_0(\beta r_2)Y_1)(\beta r_1) - J_1(\beta r_1)Y_0(\beta r_2)]$, and $\beta^2 = (\omega^2 - i\omega k)/gh$, $\omega = 2\pi/T$, r_1 and r_2 = inner and outer radii, respectively, where J_p and Y_p are the Bessel functions of the first and second kinds, respectively, of order p; $i = \sqrt{-1}$; ω the angular frequency; h_0 is the water depth and k is the linear bottom friction coefficient.

The grid configuration shown in Fig. 1 is used to test the model. The inner (r_1) and outer (r_2) radii are kept, respectively, as 47,800 and 85,400 m. The amplitude (ζ_0) of the sinusoidal wave is 0.5 m, $T = 12.42$ h, and the depth of the configuration is kept constant at 10 m. Figs. 2(a) and (b) show, respectively, a comparison of the observed and model predicted surface elevations and radial velocities at maximum conditions, for a model time step of 600 s. The errors in the model predicted surface elevations are less than 0.8% and the maximum error was found to occur near the inner radius. The maximum error in the radial velocity of 2.5% was also found to occur near the inner radius. The error in the model predicted surface elevations and velocities remained the same for a model time step of 1200 s. The model predicted current pattern clearly reproduced the radial symmetry exhibited by the analytical solution.

6.2. Residual flow

The ability of the model to predict residual flow was tested for a rectangular basin using constant vertical viscosity and density. Taking the case of a closed rectangular channel, with constant depth, model tests were performed for (i) constant surface wind stress and (ii) longitudinal density gradient as

forcing functions. Neglecting the advection, Coriolis, and horizontal diffusion of momentum, the steady-state expression for the vertical distribution of longitudinal velocities can be derived following Officer (1976) as

$$u = gi\left\{\frac{z^2}{2A_v} - \frac{h}{k} - \frac{h^2}{2A_v}\right\} - \frac{g\lambda}{\rho}\left\{\frac{z^3}{6A_v} + \frac{h^2}{2k} + \frac{h^3}{6A_v}\right\} + \frac{\tau_s}{\rho}\left\{\frac{z}{A_v} + \frac{1}{k} + \frac{h}{A_v}\right\}. \quad (18)$$

The expression for surface slope would be

$$gi = \frac{-g\lambda/\rho\{h^4/8A_v + h^3/2k\} + \tau_s/\rho\{h^2/2A_v + h/k\}}{h^3/3A_v + h^2/k}, \quad (19)$$

where λ is the horizontal density gradient, g the gravity, i the water surface slope, h the water depth, k the linearized bottom friction coefficient, τ_s the

Table 1
Range of grid angles for the grid

Range of grid angle	No. of grid cell corners
30–40°	4
40–50°	78
50–60°	248
60–70°	1489
70–80°	4580
80–85°	4388
85–90°	7347

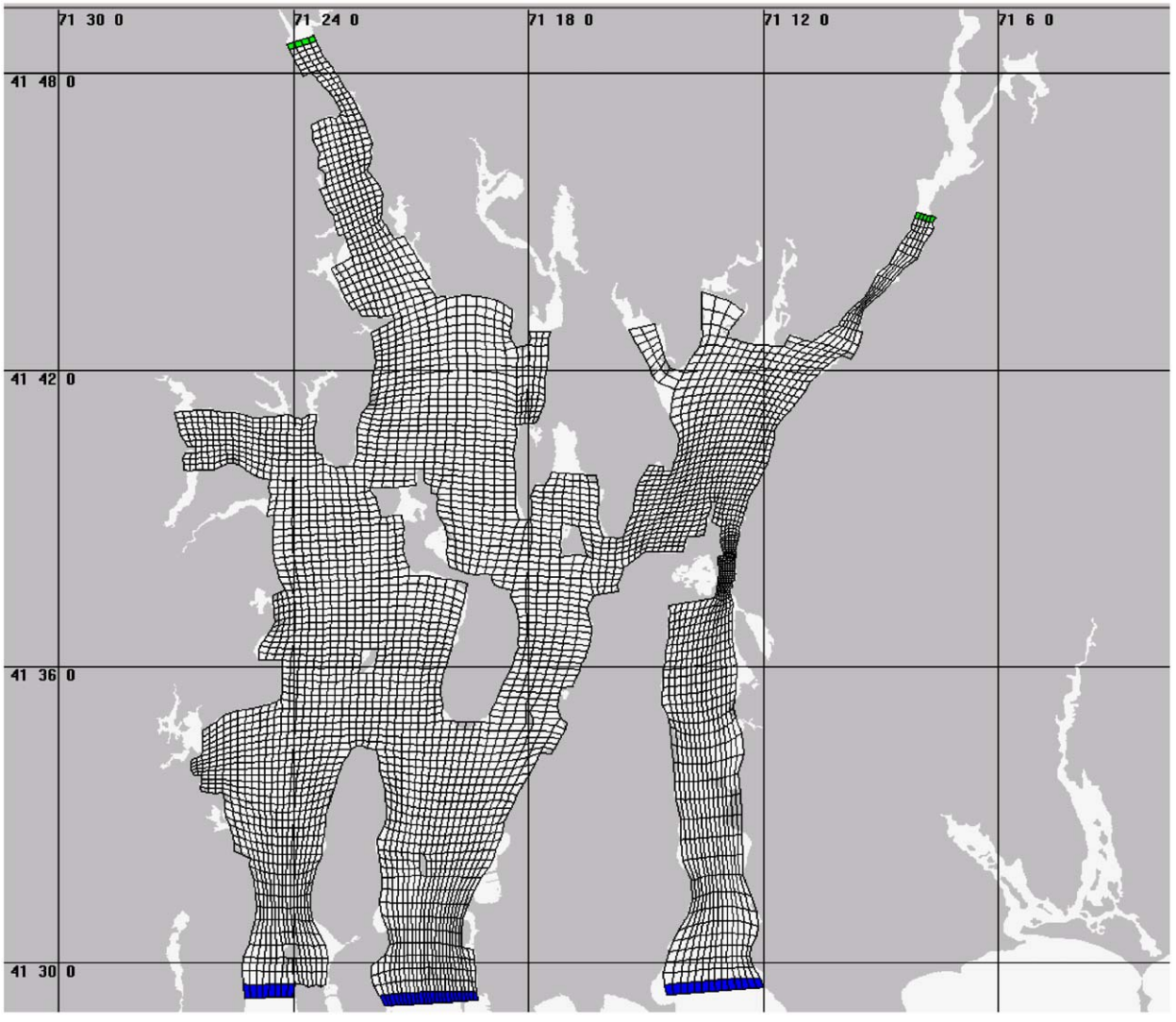

Fig. 5. Grid for the study area.

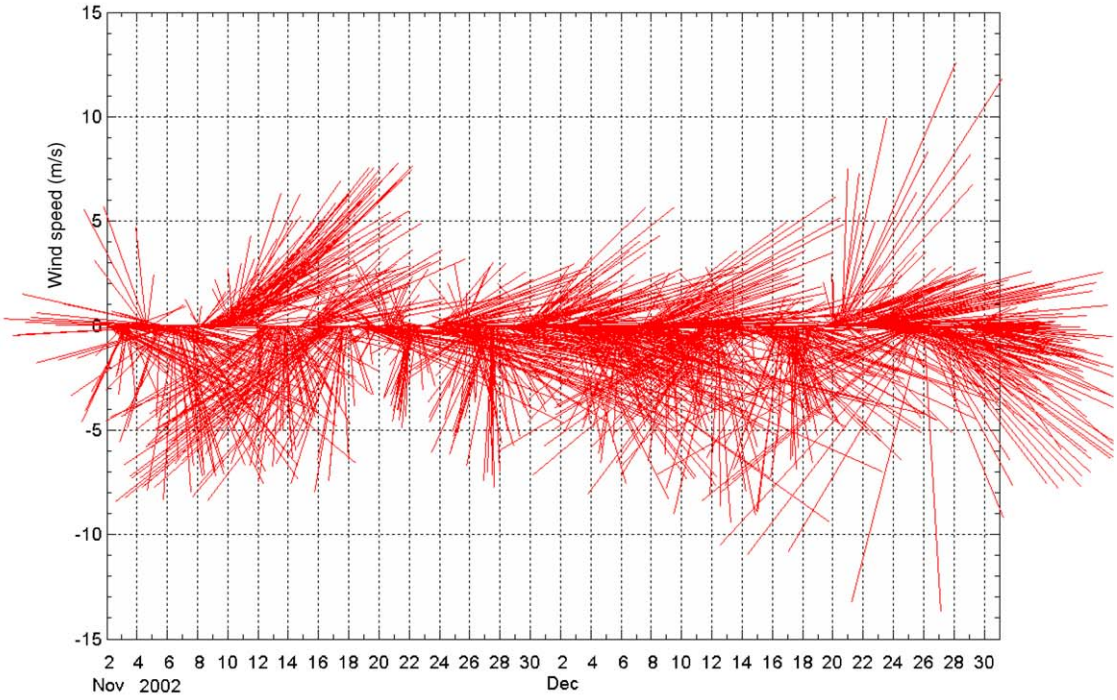

(a)

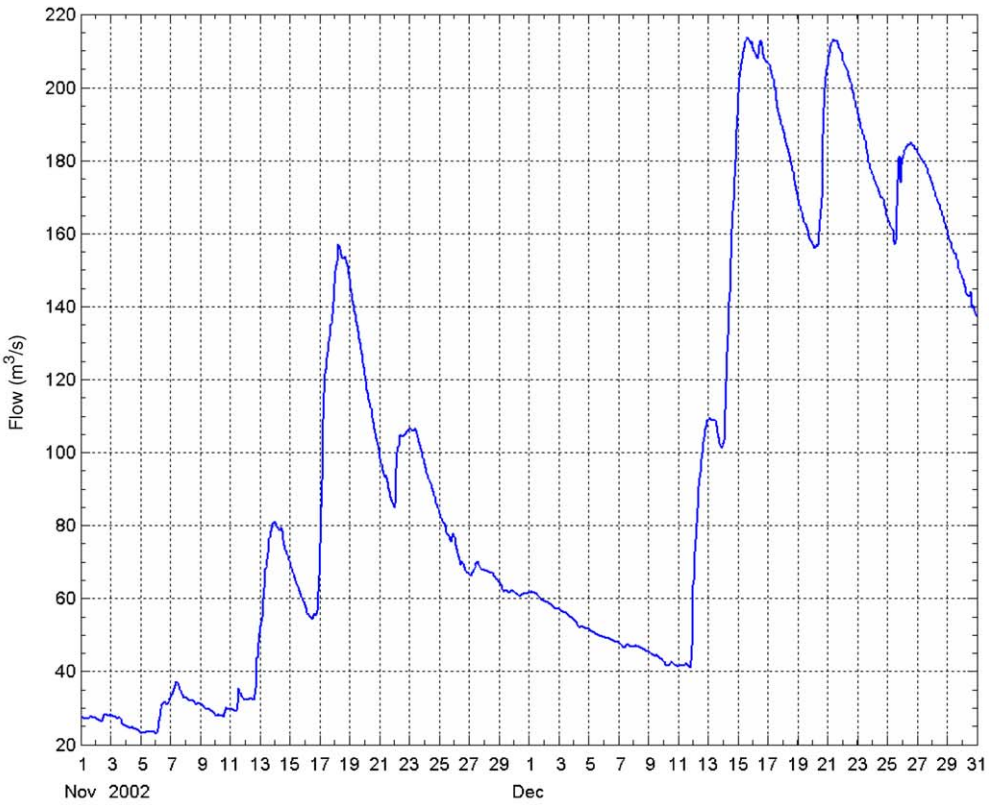

(b)

Fig. 6. (a) Observed wind records at Providence airport. (b) Hourly freshwater flows into Narragansett Bay.

surface wind stress and A_v is the vertical eddy viscosity.

6.3. Wind forcing

The residual circulation in an 11 m deep basin, induced in by a uniform wind stress of 0.182 N/m^2 applied at the surface, equivalent to a wind speed of 10 m/s is computed using the model. Assuming a vertically constant eddy viscosity of 0.001 m^2/s and keeping the bottom friction coefficient to be 0.001 m/s, the model predicted vertical distribution of longitudinal velocities, using 11 equal vertical layers, compares well with the analytical solution as shown in Fig. 3(a) and the error in the model predicted velocities are less than 4.2%.

6.4. Density gradient forcing

The seaward flow of river water at the head of the estuary causes a density gradient between the fresh water at the head of the estuary and sea water at the mouth of the estuary. The longitudinal density gradient caused due to this density difference plays a

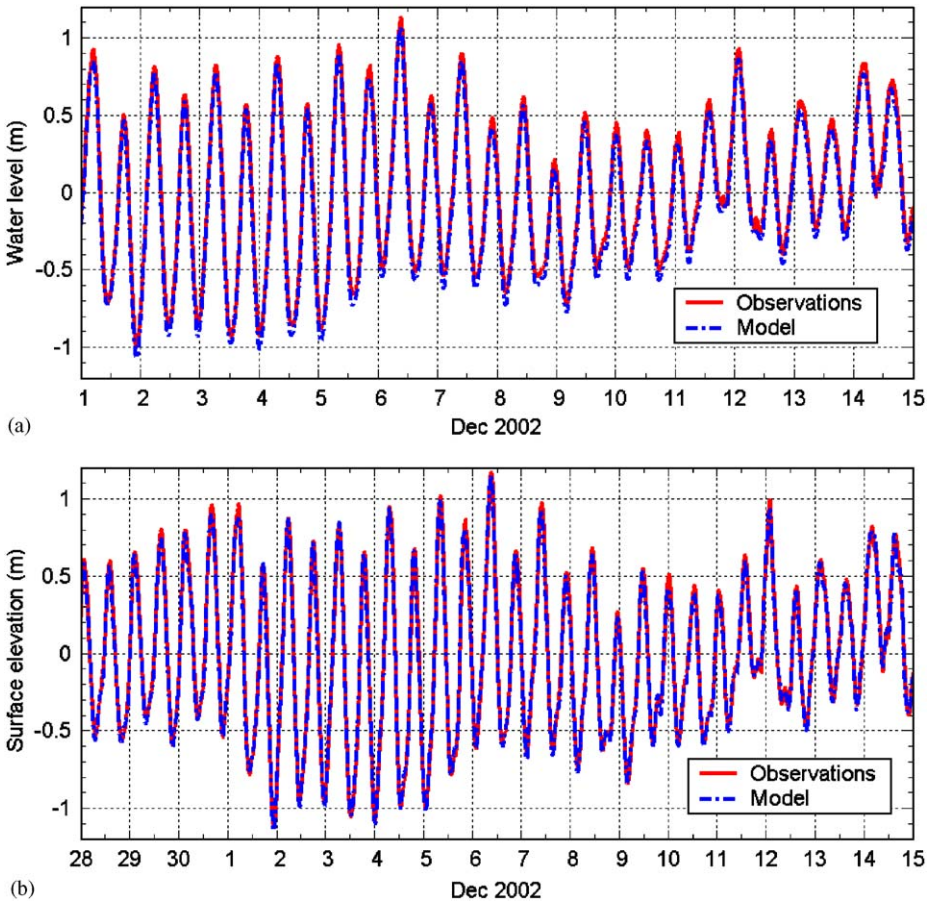

Fig. 7. (a) Comparison of Observed and model predicted surface elevations at Quonset. (b) Comparison of observed and model predicted surface elevations at Conimicut.

Table 2
Statistical evaluation of model performance for instantaneous elevations

Station	Number of data points	Data range (m)	RMS error (m)	RMS error (%)	Correlation coefficient
Quonset Point	4081	2.132	0.064	3.0	0.999
Conimicut	4081	2.293	0.043	1.87	0.997

major role in the estuarine circulation pattern. The circulation induced by a constant density gradient is simulated using the present model and compared with that obtained using the analytical solution given by Eqs. (18) and (19) Assuming the density to be vertically constant, the density varies from 1000 to 1025 kg/m^3 over a distance of 23 km. The steady-state vertical distribution of longitudinal velocities obtained using the model, using a vertical eddy viscosity of 0.001 m^2/s and linearized bottom friction coefficient as 0.001 m/s compares well (Fig. 3b) with the analytical solution given by Eq. (18). The errors in the model predicted velocities are less than 7%.

7. Application of the model to study the circulation in Narragansett Bay

Narragansett Bay (Fig. 4) is composed of four major passages, West Passage, East Passage, Providence River and Sakkonet River and has a mean depth of 9 m. The tidal wave enters Narragansett Bay from Rhode Island Sound through the East and West Passages and the Sakkonet River. The tide is predominantly semi-diurnal with standing wave characteristics. Haight (1936) found that the interactions between M_4, M_6 and M_2 tides result in double peaked flood currents profiles commonly seen in Narragansett Bay. A detailed description about the tidal hydrodynamics within Narragansett Bay can be found in Haight (1936) and Ward and Spaulding (2001). A detailed account of the non-tidal circulation in Narragansett Bay is given in Weisberg and Sturges (1976).

Many circulation models have been applied to Narragansett Bay, however most focused primarily on tide and wind driven flows and neglected the effects of density driven flows. For example, Gordon and Spaulding (1987) investigated the tidal and wind-driven circulation in Narragansett Bay using a three-dimensional rectangular coordinate hydrodynamic model. Muin and Spaulding (1997b) applied a three-dimensional boundary-fitted hydrodynamic model to study the circulation in Providence River. Ward and Spaulding (2001) calibrated and validated a two-dimensional vertically averaged hydrodynamic model that served as a core of a nowcast/forecast system of circulation dynamics for Narragansett Bay. Ward (1999) developed a depth averaged finite volume shallow water model using

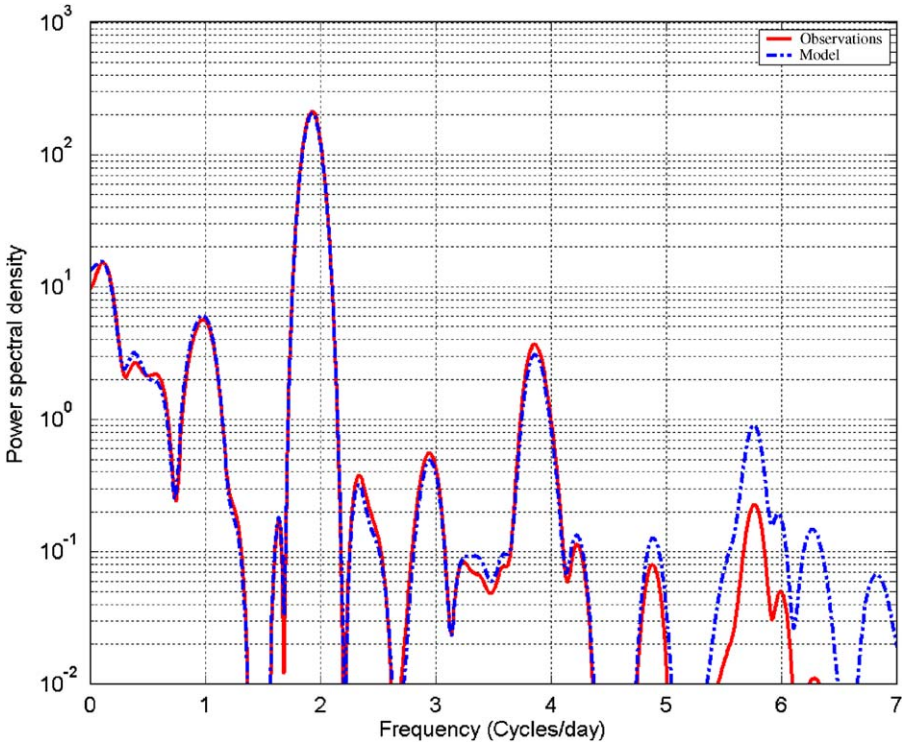

Fig. 8. Comparison of power spectra of model predictions to observations for surface elevation at Conimicut Point during November–December 2002.

triangular elements and applied it to study the circulation in Narragansett Bay.

The three-dimensional hydrodynamic model developed in the present study, taking density driven flows into account, is applied to model circulation and transport within Narragansett Bay. A detailed skill assessment of the model is performed, by comparing the model-predicted surface elevations, currents, salinities, and temperatures, with observations.

7.1. Model grid

The model study area and its bathymetry is shown in Fig. 4. The grid of the model study area (Fig. 5), consists of 95×210 segments with 4585

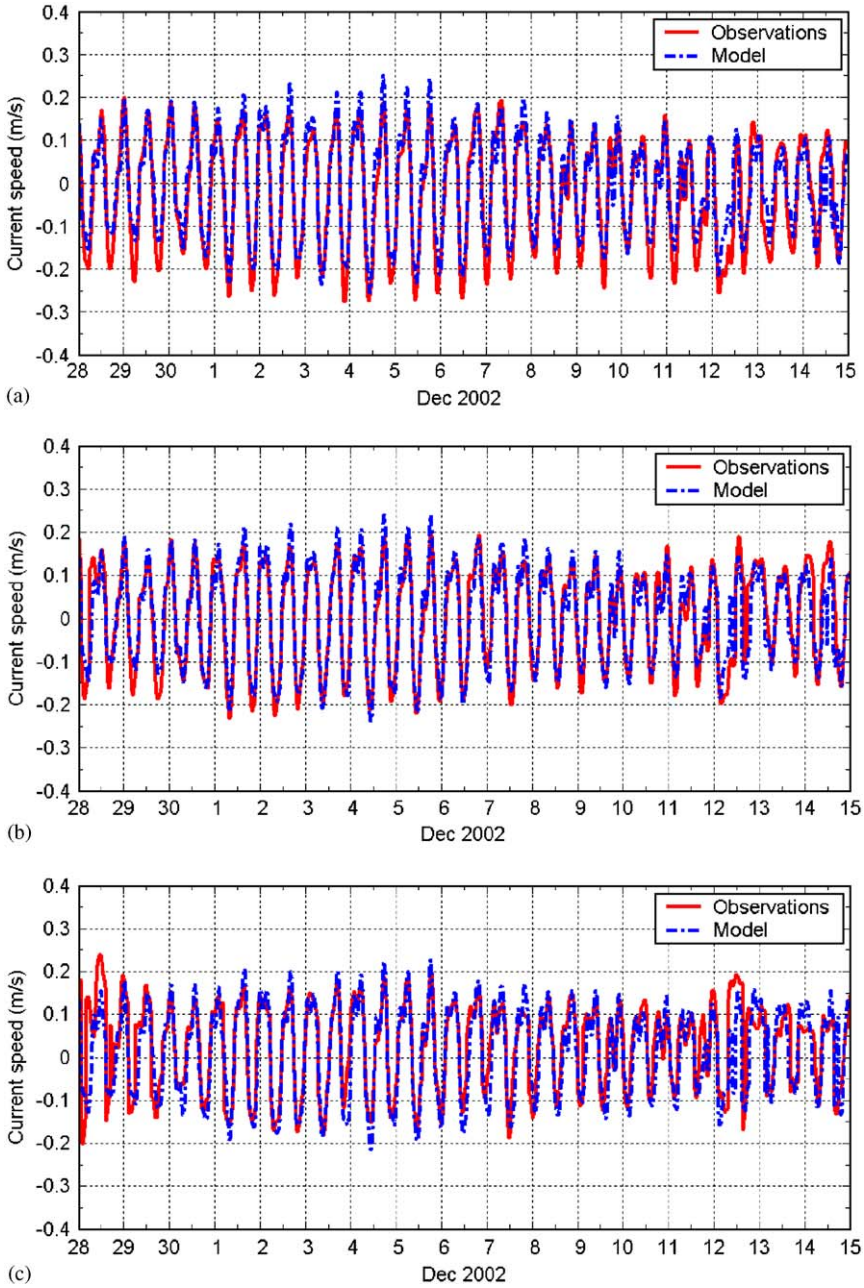

Fig. 9. Comparison of the observed and model-predicted current speeds at a ADCP station in the Quonset Channel 1–16 December 2002. (a) Near surface (8 m) from bottom. (b) Near mid-depth (5 m from bottom). (c) near bottom (2 m from bottom).

cells. A set of Poisson partial differential equations with Dirichlet boundary conditions (Thompson et al., 1985) is employed to generate the boundary fitted grid. Grid non-orthogonality was significantly reduced by judiciously moving the boundary points and by the use of interior control points. Table 1 gives a summary of the skewness of the grid cell corners for the boundary-fitted grid shown in Fig. 5. A grid angle of 90° represents an orthogonal grid. It is seen that 90% of the grid cell corners have grid angles greater than 70°. Eleven sigma layers of equal thickness are used in the vertical. Bathymetric soundings with associated latitude and longitude for the area were accessed from National Geophysical Data Center NGDC (1996) and the bathymetry was then mapped onto the computational grid.

7.2. Model boundary conditions

The tide height or free surface elevation recorded at 6 min intervals by National Ocean Survey (NOS) tide gauge station at Newport, RI was obtained and filtered using a 3-h low pass filter and were used along the three ocean open boundaries at the southern end of the study area. No significant changes in amplitude or phase occur across these three boundaries. Surface water temperatures measured at Newport by NOS were forced along the

Table 3
Statistical evaluation of model performance at the Quonset ADCP station in the Quonset Channel

Depth from bottom (m)	RMS error (m/s)	Data range (m/s)	RMS error (%)	Correlation coefficient
3	0.057	0.444	12.9	0.860
4	0.047	0.414	11.3	0.910
5	0.040	0.431	9.3	0.940
6	0.038	0.449	8.4	0.954
7	0.043	0.476	9.0	0.951
8	0.062	0.582	10.7	0.917

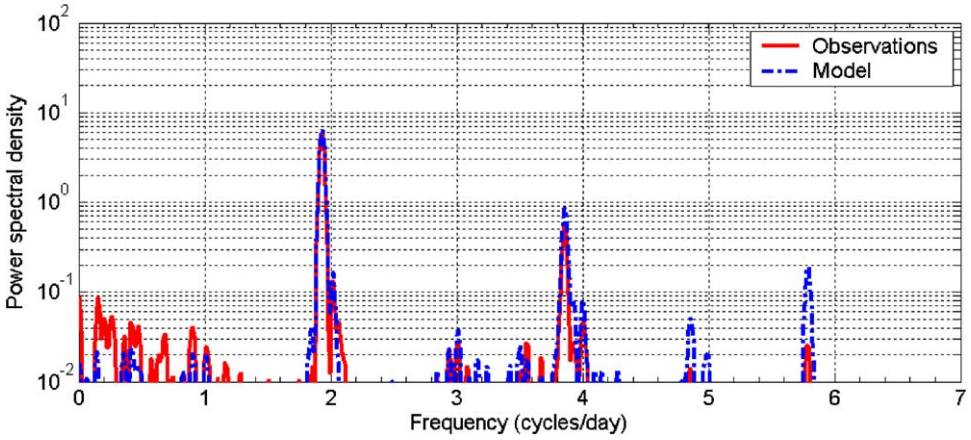

Fig. 10. Comparison of power spectra of observations and model predictions at mid-depth at ASA ADCP station.

Table 4
Properties of observed M_2 and M_4 current harmonics

	M_2 amplitude (m/s)	M_4 amplitude (m/s)	Ratio of amplitudes M_4/M_2	Phase of M_2 ϕ_{M_2} (°)	Phase of M_4 ϕ_{M_4} (°)	$2\phi_{M_2} - \phi_{M_4}$
2	6.6	2.5	0.379	144.2	9.8	278.6
5	13	4	0.308	129.3	46.3	212.3
8	16.7	4.1	0.246	136.3	58.5	214.1

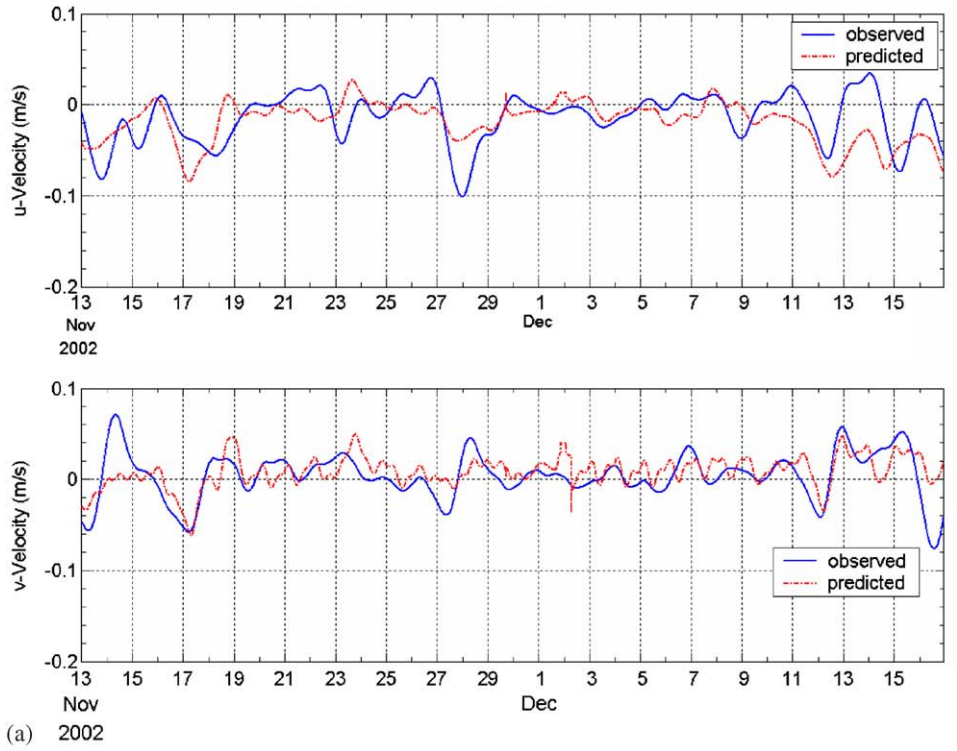

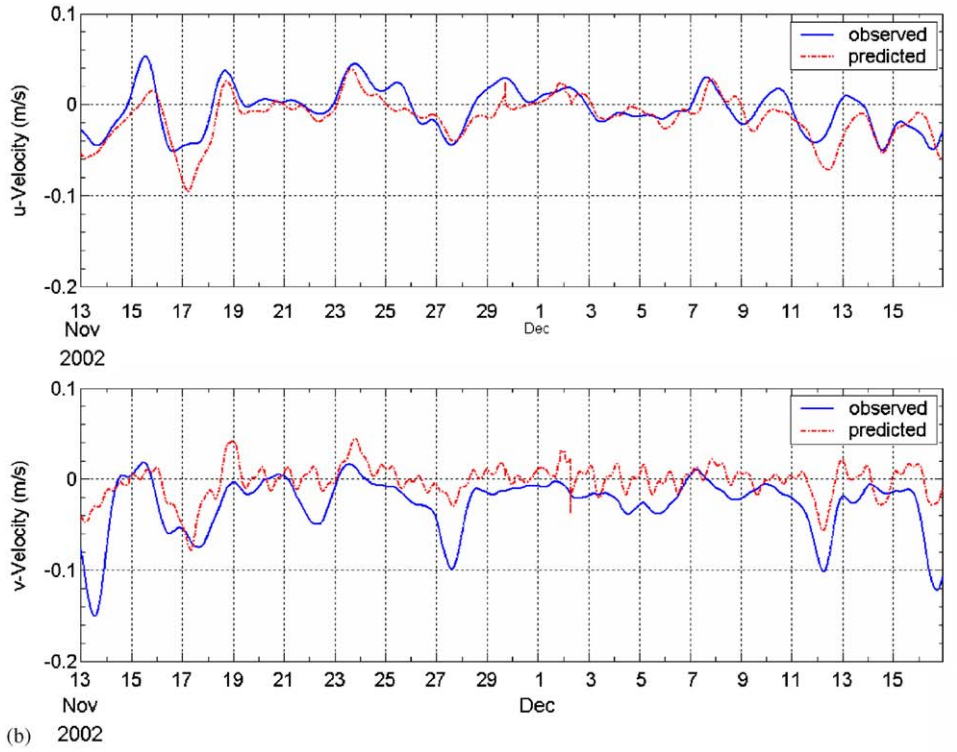

Fig. 11. (a) Comparison of observed and predicted 32-h low-passed u and v velocities near bottom (3 m from the bottom). (b) Comparison of observed and predicted 32-h low-passed u and v velocities near mid-depth (6 m from the bottom). (c) Comparison of observed and predicted 32-h low-passed u and v velocities near bottom (2 m from the surface).

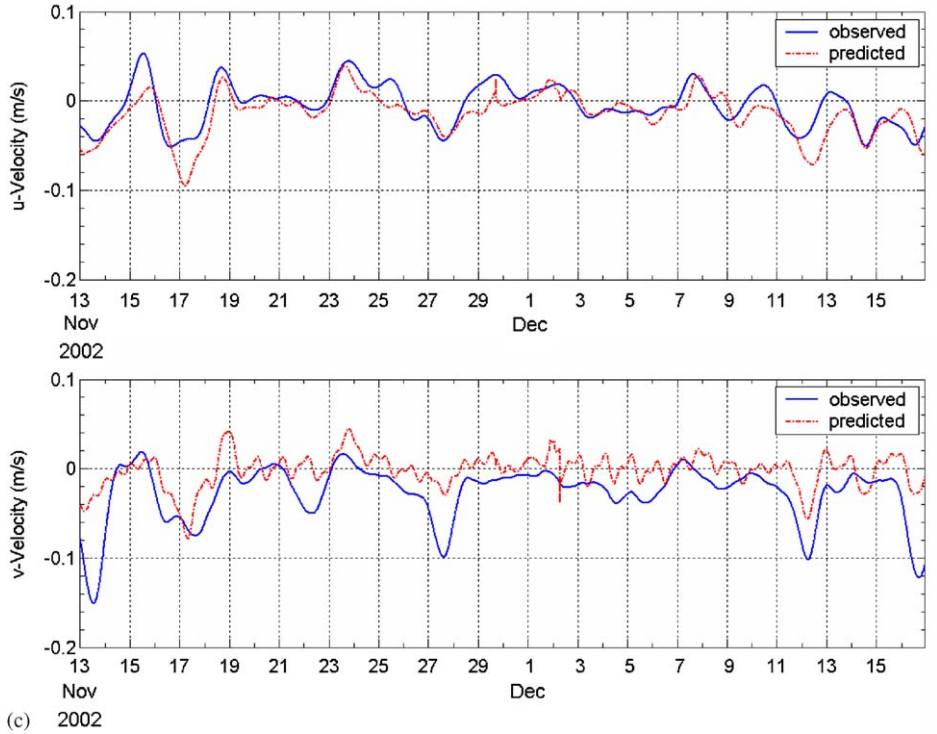

Fig. 11. (*Continued*)

open ocean boundary, while the salinity along the open boundary was held constant at 33 psu. Winds, solar radiation, atmospheric pressure, air temperature, dewpoint, and relative humidity, recorded at Green Airport in Warwick, RI were obtained from Northeast Regional Climate Center at Cornell University and used as the forcing at the air–sea interface. Fig. 6(a) shows a stick plot of the observed wind records at Providence Airport, during Nov–-Dec 2002. A quadratic wind stress coefficient of 0.0014 was used to calculate the wind stress, which was then applied uniformly over the whole study area. The total freshwater water flow into the Upper Narragansett and Mount Hope Bays were obtained from the United States Geological Survey gauging stations and used as the river forcing, after being scaled according to Ries (1990). Fig. 6(b) shows a time series plot of the total fresh water flow into the Bay during Nov–Dec 2002. A constant quadratic bottom friction coefficient of 0.003 was used in the model after preliminary testing.

8. Skill assessment of model predictions

A statistical evaluation of the model-predicted surface elevations, currents, salinity and temperature in Narragansett Bay, is done by comparing it with observations.

8.1. Surface elevations

The model-predicted surface elevations for a 29-day period compare well with the observations from NOS stations located at Quonset and Conimicut Point as shown in Figs. 7(a) and 7(b). The observed spring–neap tidal cycles and low-frequency fluctuations in the surface elevation are well reproduced by the model.

A statistical evaluation of the model performance is given in Table 2. The predicted surface elevations show excellent comparison with observations with a root mean square error of less than 3% and correlation coefficients higher than of 0.997. It is seen from Fig. 8 that the model clearly reproduces the spectral energy distributions seen in the observations at the tidal and sub-tidal frequencies.

8.2. Currents

The model-predicted current speeds at surface, mid-depth, and bottom show very good agreement

with the observations at the Acoustic Doppler Current Profilers (ADCP) station as shown in Fig. 9. The model clearly reproduces the spring and neap cycles, the shorter duration but stronger ebb dominant currents, and the double flood phenomena seen in the observations. Friedrichs and Aubrey (1988) showed that when M_4 is locked in a velocity phase of 90–270°, with respect to M_2, the distorted composite tide has higher ebb current and larger the M_4/M_2 amplitude ratio, the more ebb-dominant is the tidal current. The observed M_2 and M_4 tidal current harmonic characteristics at surface and mid-depth, given in Table 4, clearly explain the ebb dominance seen in observed tidal currents (Figs. 9(i) and (ii)) at Quonset.

A statistical evaluation of the model-predicted three-dimensional current speeds at the ADCP station is given in Table 3. The root mean square (RMS) errors of the model predictions are less than 13% of the maximum speeds and correlation coefficients exceed 0.860. The current power spectra for the observations and model predictions at mid-depth at the ADCP location is shown in Fig. 10. It is seen that the model predictions clearly reproduce the energy spectral levels seen in the observations, particularly for the M_2 and M_4 periods (Table 4). However, the model does not reproduce the low-frequency currents very well (Fig. 10), even though it reproduces the low-frequency surface elevations very well (Fig. 8). This can be attributed to the fact

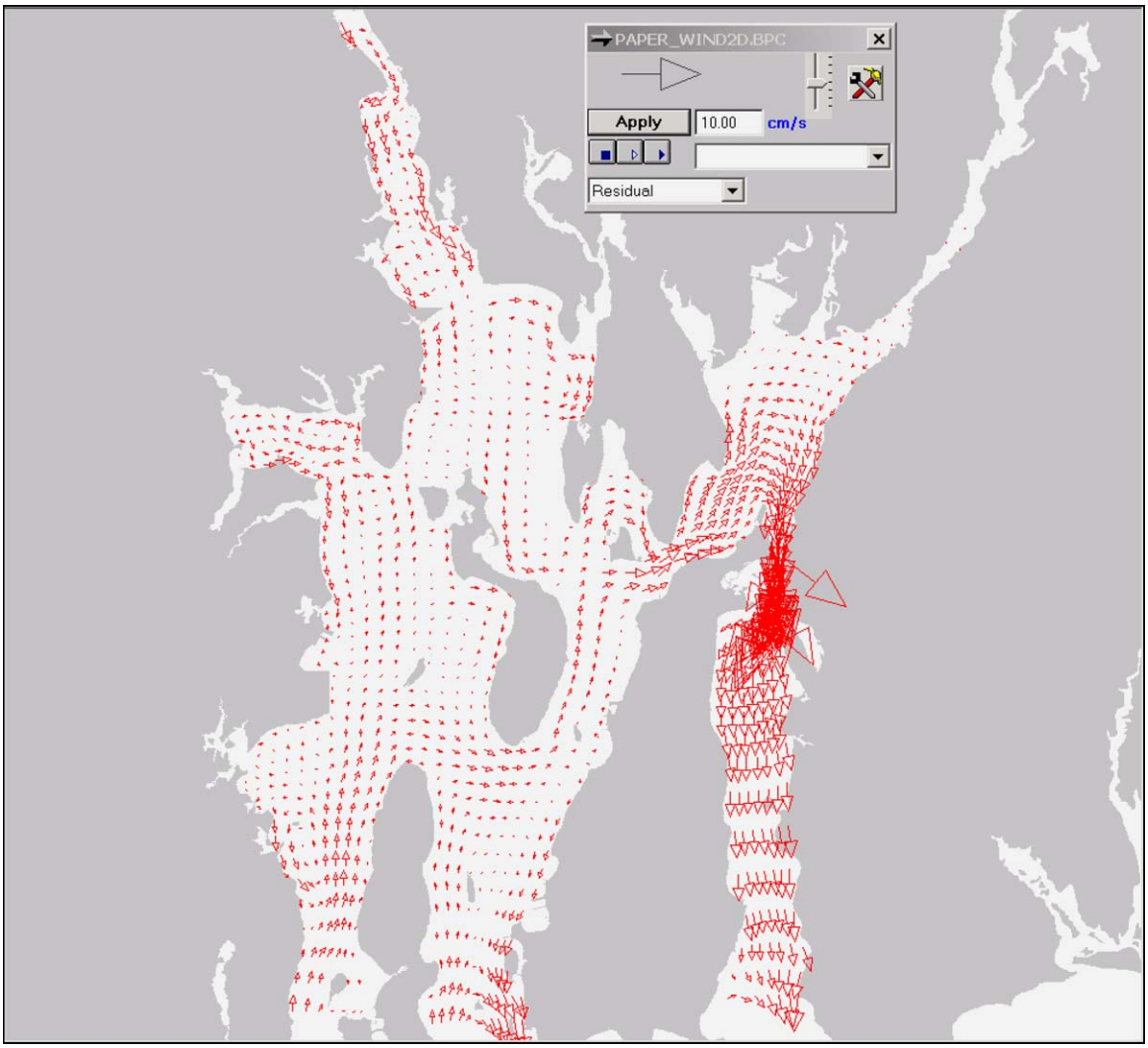

Fig. 12. Wind-driven residual circulation, averaged over 60 days at the bottom (1 m from the bottom), with model forcing due to winds only. The current vectors are plotted at every other cell.

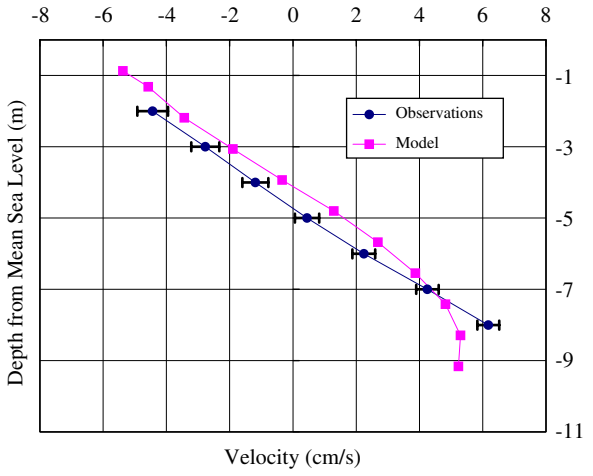

Fig. 13. Comparison of observed and predicted mean currents along the vertical.

that the only surface elevations are forced along the open boundaries and the circulation due to non-local forcing from the offshore is not taken into account. The observed and predicted 32-h low-passed currents at the bottom (Fig. 11a), mid-depth (Fig. 11b), and surface (Fig. 11c) compares well for the most-part.

8.3. Residual currents

Residual currents could be generated due to non-linearity in the dynamics of tidal flow (Signell and Geyer, 1991), local wind stress on the surface (Rady et al., 1998), and longitudinal density gradient (Weisberg and Sturges, 1976). The magnitudes of the residual current speeds are usually smaller than the tide and wind-induced currents.

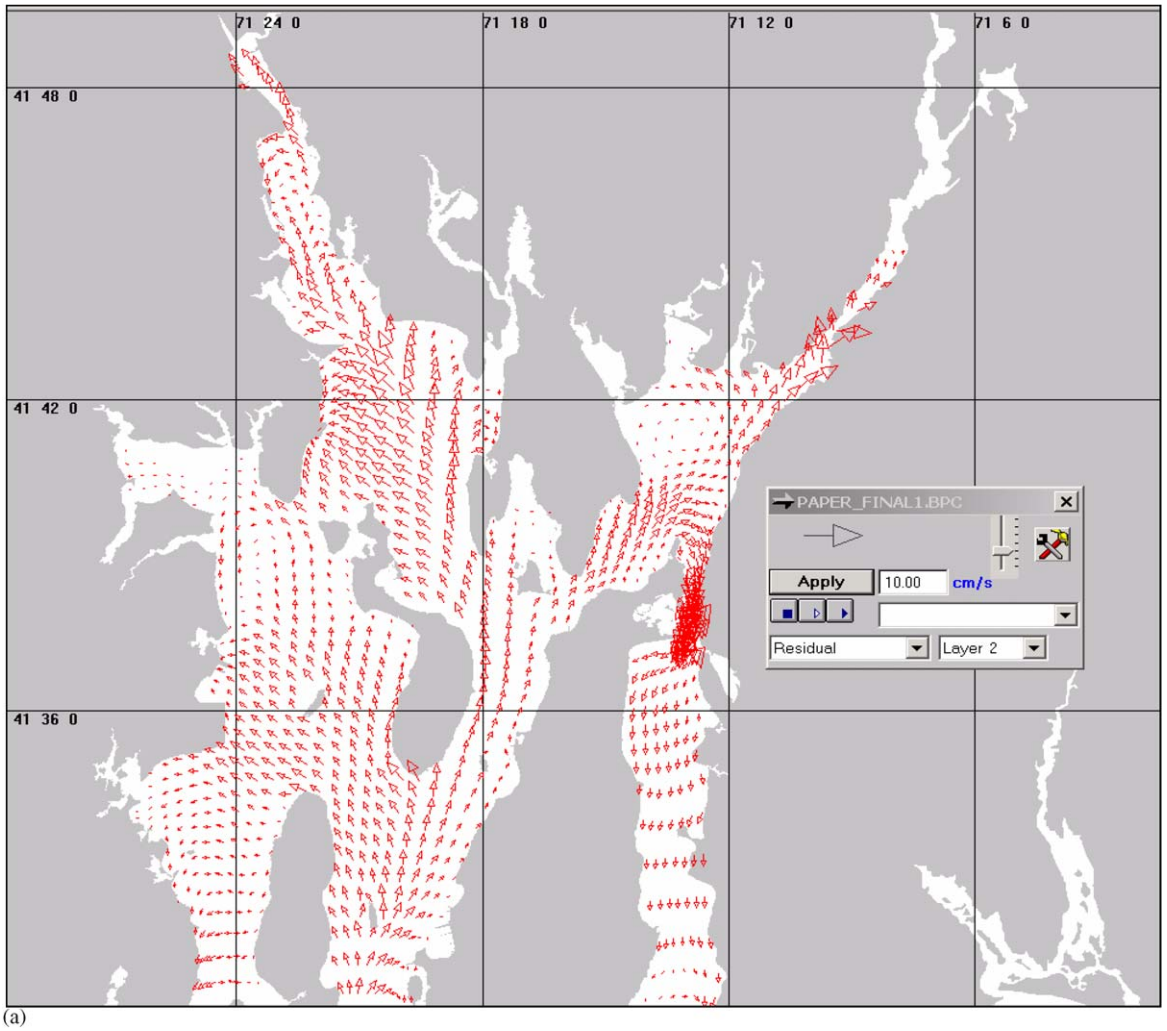

(a)

Fig. 14. (a) Residual circulation, averaged over 60 days at the bottom (1 m from the bottom). The current vectors are plotted at every other cell. (b) Residual circulation, averaged over 60 days at the surface (0.5 m from the surface). The current vectors are plotted at every other cell.

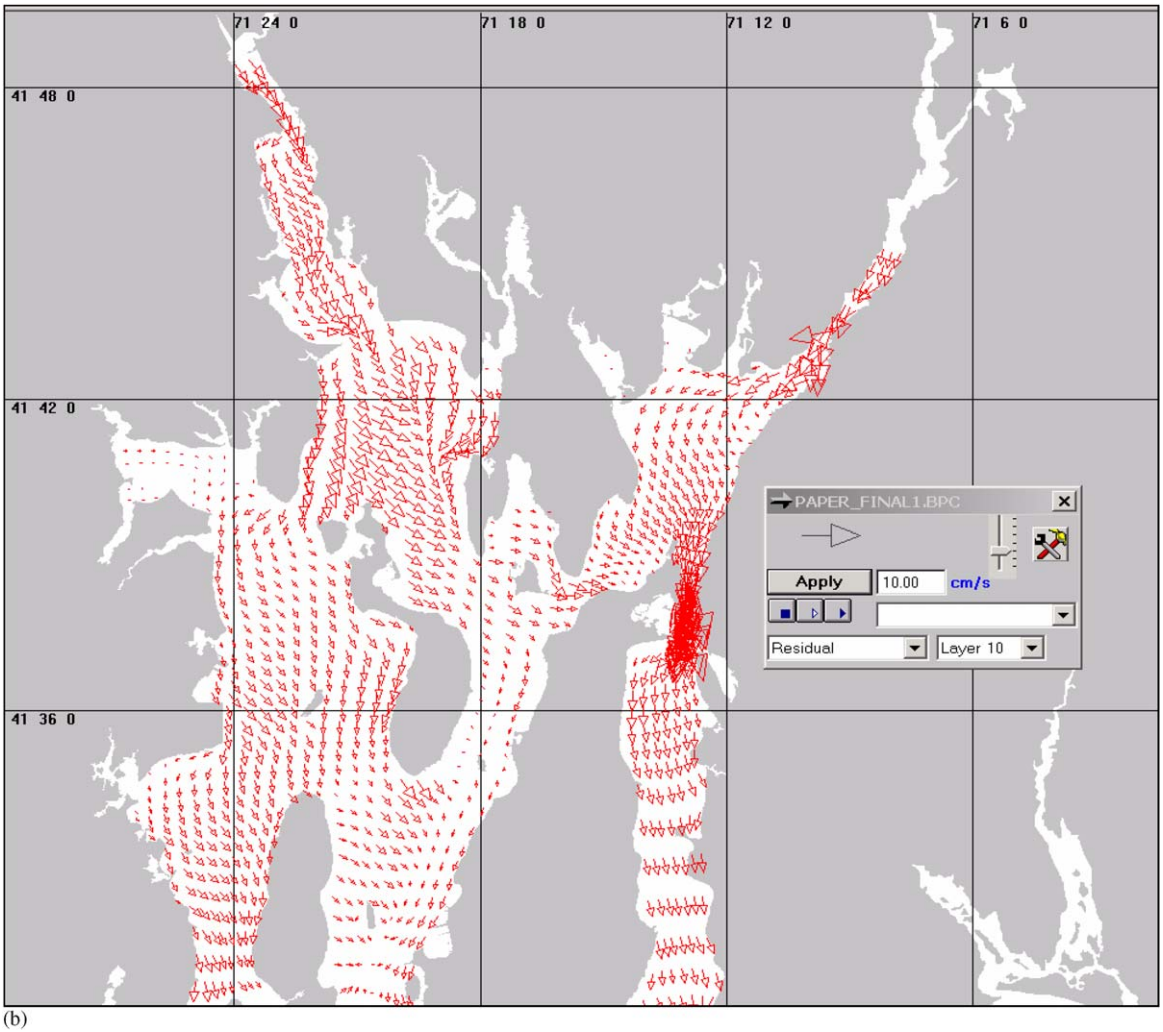

(b)

Fig. 14. (*Continued*)

The model-predicted residual currents presented in this study were obtained by taking a time-average of the model-predicted instantaneous currents, over at least 1-month period.

Residual mean currents presented in this study were obtained by time-averaging the model-predicted and observed currents over the 60-day period (November–December 2001). The model predicted tide induced residual currents in the Bay were seen to be very small, with maximum tide-induced residual currents of 1 cm/s in the Sakknonet passage. The model predicted depth-averaged wind-induced residual currents vary between 1 and 10 cm/s (Fig. 12) with maximum currents of 10 cm/s in the Sakonnet River. Fig. 13 shows a comparison of the observed and predicted mean currents along the vertical. Figs. 14 (a) and (b) show the total residual mean currents in the surface and bottom, respectively. It is seen that the model clearly reproduces the estuarine flow, with a landward flow (Fig. 14a) at the bottom and a seaward flow at the surface (Fig. 14b). It is to be noted that the residual currents due to winds dominates over the estuarine flow in the Sakonnet River (Fig. 14(a)).

8.4. Salinity and temperature

The model predicted salinities were found to be insensitive to variations in the horizontal dispersion coefficient and was kept at 100 cm^2/s. The vertical diffusion coefficient was varied from 6 to 20 cm^2/s and the best match between the observed and predicted salinities was obtained using a value of 10 cm^2/s.

Fig. 15 shows the comparison of the observed and model-predicted salinities at the surface, mid-depth and bottom at Quonset. The model clearly reproduces the non-tidal salinity variations at the bottom and mid-depth, but somewhat over estimates them at the surface. The tidal variation of the salinity is often overestimated. A statistical evaluation of the model-predicted salinities is given in Table 5. The error in the time-averaged mean salinity between the model predictions and observations is 0.1 psu at the bottom and mid-depth, and 0.7 psu at the surface.

Fig. 16 shows a comparison of the observed and model predicted temperatures at Quonset. The model clearly reproduces the non-tidal variations of temperatures seen in the observations. A statistical evaluation of the model predicted temperature is given in Table 6.

9. Summary and conclusions

A three-dimensional, orthogonal coordinate semi-implicit hydrodynamic model in spherical

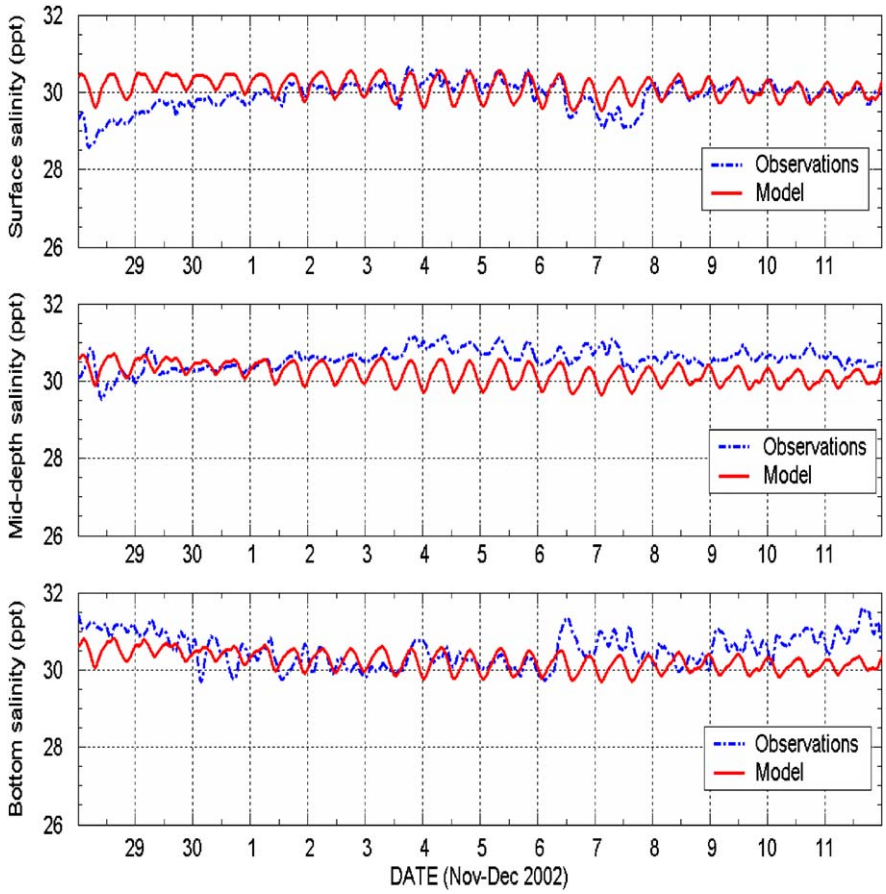

Fig. 15. Comparison of observed and predicted salinities at surface, mid-depth and bottom at Quonset.

Table 5
Statistical evaluation of the observed and predicted salinities_Toc63487026 at Quonset station

Instrument depth	RMS error (psu)	Time averaged mean salinities		Correlation coefficient
		Observed (psu)	Model (psu)	
Near bottom	0.453	29.917	30.121	0.998
Mid-depth	0.537	30.568	30.194	0.990
Near surface	0.559	30.525	30.235	0.950

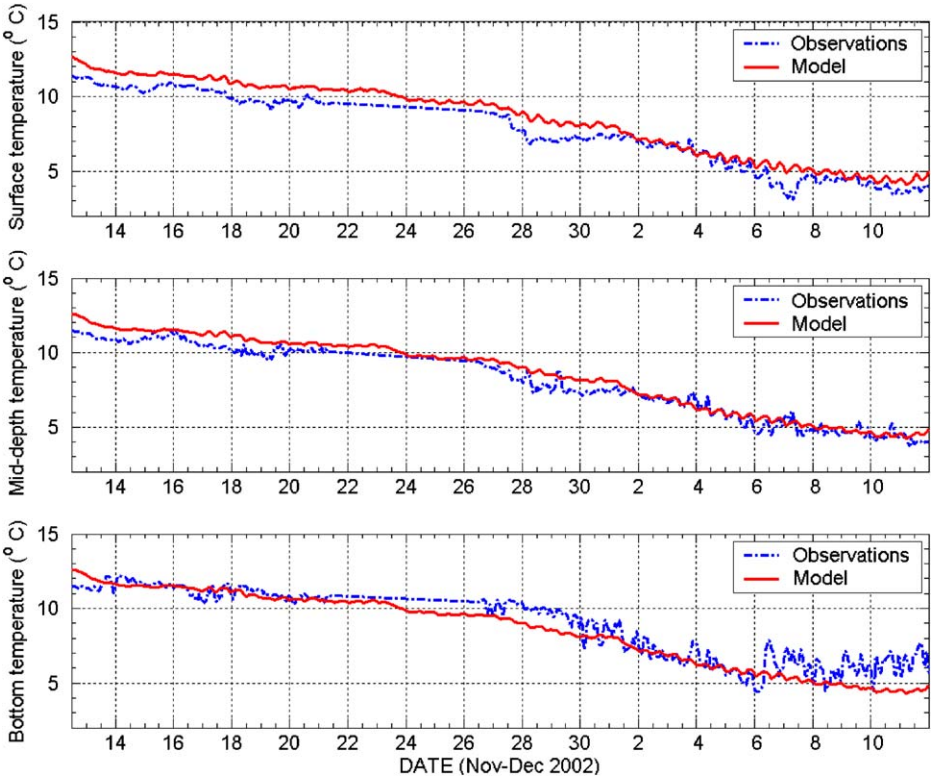

Fig. 16. Comparison of observed and predicted temperatures at surface, mid-depth and bottom at Quonset.

Table 6
Statistical evaluation of the observed and predicted temperatures at Quonset station

Instrument depth	RMS error (°C)	Time averaged mean temperatures		Correlation coefficient
		Observed (°C)	Model (°C)	
Near bottom	0.846	7.493	8.229	0.988
Mid-depth	0.622	7.822	8.282	0.990
Near surface	0.966	8.785	8.300	0.950

coordinates that can be applied to estuarine, coastal sea and continental shelf waters is presented. A generalized orthogonal coordinate transformation on the horizontal and a sigma coordinate transformation on the vertical, are applied to the governing equations. The governing equations are decomposed into exterior and interior modes and solved using a semi-implicit solution technique. Second-order accurate spatial and temporal discretization schemes are used on a space-staggered grid. A simple flooding and drying technique is used to model the tidal flats.

The model results are tested against analytical solutions for tidal circulation in an annular channel and steady residual flow generated by wind, and density differences in a rectangular channel. The predictions from the model showed very good comparison with analytical solutions for all the test cases.

Three-dimensional circulation in Narragansett Bay was then studied using the developed model. The model forcing functions consist of meterological data, water elevation, salinity, and temperature along the open boundary, and freshwater inflows from two major rivers. The model predicted surface elevations, three-dimensional instantaneous and mean currents, salinities, and temperatures in Narragansett Bay are compared with the observations. Mean errors in the

model predicted surface elevations and velocities are less than 3% and 15%, respectively. The model clearly reproduces the spring and neap cycles, the shorter duration but stronger ebb dominant currents and the double flood phenomena seen in the observations. Correlation coefficients for salinity and temperatures exceed 0.95 and 0.87, respectively. The mean estuarine currents, and the sub-tidal currents seen in the observations are clearly reproduced by the model.

The skill assessment of the model clearly showed the capability of the model to predict the surface elevation, currents, salinities and temperature at tidal and sub-tidal frequencies.

We plan to incorporate the eta-coordinate system (Luo et al., 2002) that can be applied to problems with steep bottom slopes, and a turbulence closure scheme (Mellor and Yamada, 1974) that can be applied to highly stratified systems in the model presented in this study.

Acknowledgement

We acknowledge and greatly appreciate the reviewers' comments, which helped to significantly improve and strengthen this manuscript.

Appendix A

A.1. Symbols

U, V	vertically averaged velocities
ξ, η	general orthogonal coordinate system
ζ	surface elevation
ρ_0	mean water density of water
ρ_a	density of air
f	coriolis parameter $= 2\Omega \sin\phi$
Ω	angular velocity of earth
S	salinity
T	temperature
D_h, D_v	horizontal and vertical diffusivities
A_v	vertical eddy viscosity
D	total water depth $(h+\zeta)$
g	acceleration due to gravity
R	radius of the earth.
σ	sigma coordinate system $\left(\sigma = \frac{z-\zeta}{H+\zeta}\right)$
ϕ, θ	longitude, latitude
C	concentration (salt or temperature)
J_p	Bessel functions of the first kind of order p;
Y_p	Bessel functions of the second kind of order p;
i	$\sqrt{-1}$
ω	angular frequency
τ	linear bottom friction coefficient.
u', v'	deviations of the three-dimensional velocities in ϕ and θ directions
ω	velocities normal to the sigma level

$$g_{11} = \left(\frac{\partial\phi}{\partial\xi}\right)^2 \cos^2\theta + \left(\frac{\partial\theta}{\partial\xi}\right)^2,$$

$$g_{22} = \left(\frac{\partial\phi}{\partial\eta}\right)^2 \cos^2\theta + \left(\frac{\partial\theta}{\partial\eta}\right)^2.$$

Appendix B

B.1. Derivation of scale factors in spherical coordinate system

The position vector on the surface of the sphere (ϕ,θ, R = constant) is given by

$$\hat{r} = (R\ \cos\ \theta)\phi\hat{e}_\phi + R\theta\hat{e}_\theta, \tag{B.1}$$

where ϕ is the longitude, θ is the latitude R is the radius of the earth and $\hat{e}_\phi$ and $\hat{e}_\theta$are the curvilinear unit vectors in ϕ and θ directions, respectively.

The derivatives of the position vectors in the (ξ,η) directions are given by

$$\hat{g}_1 = \frac{\partial\hat{r}}{\partial\xi} = R\ \cos\ \theta\phi_\xi i + R\theta_\xi j, \tag{B.2}$$

$$\hat{g}_2 = \frac{\partial\hat{r}}{\partial\eta} = R\cos\theta\phi_\eta i + R\theta_\eta j, \tag{B.3}$$

where i and j are the unit vectors ξ, η directions and the subscripts in the equations indicate partial derivatives $\left(\phi_\xi = \frac{\partial\phi}{\partial\xi}\right)$.

Normalizing with respect to R, since R is constant on the surface of the sphere, the covariant components of the metric tensor $g_{ij} = \hat{g}_i \cdot \hat{g}_j$ are given by,

$$\begin{aligned} g_{11} &= \phi_\xi\phi_\xi \cos^2\theta + \theta_\xi\theta_\xi, \\ g_{12} &= g_{21}\phi_\xi\phi_\eta \cos^2\theta + \theta_\xi\theta_\eta, \\ g_{22} &= \phi_\eta\phi_\eta \cos^2\theta + \theta_\eta\theta_\eta. \end{aligned} \tag{B.4}$$

References

Ahsan, A.K.M.Q., Blumberg, A.F., 1999. Three-dimensional hydrothermal model of Onondaga Lake, New York. Journal of Hydroulic Engineering ASCE 125 (9), 912–923.

Aldridge, J.N., Davies, A.M., 1993. A high resolution three-dimensional hydrodynamic tidal model of the Eastern Irish Sea. Journal of Physical Oceanography 23, 207–224.

Arakawa, A., Lamb, V.R., 1977. Computational design of the basic dynamical processes of the UCLA General Circulation Model. Method in Computational Physics 17, 165–173.

Blackadar, A.K., 1962. The vertical distribution of wind and turbulent exchange in the a neutral atmosphere. Journal of Geophysical Research 67, 3095–3120.

Blumberg, A.F., 1986. Turbulent mixing processes in lakes, reservoirs, and impoundments''. In: Gray, W. (Ed.), Physics Based Modeling of Lakes, Reservoirs, and Impoundments. ASCE, New York, pp. 79–97.

Blumberg, A.F., Mellor, G.L., 1987. A description of the three-dimensional coastal ocean circulation model. In: Heaps, N. (Ed.), Three-Dimensional Coastal Ocean Models, vol. 4. American Geophysical Union, Washington, DC, 208pp.

Blumberg, A.F., Herring, H.J., 1987. Circulation modeling in orthogonal curvilinear coordinates. In: Nihoul, J.C.J., Jamart, B.M. (Eds.), Three-dimensional Models of Marine and Estuarine Dynamics, p. 269.

Blumberg, A.F., Galperin, B., O' Connor, D.J., 1992. Modeling vertical structure of open-channel flows. Journal of Hydraulic Engineering ASCE 118 (8), 1119–1134.

Chan, C.-T., Cheong, H.F., Shankar, N.J., 1994. A boundary-fitted grid for tidal motions: orthogonal coordinates generation in 2D embodying Singapore Coastal Waters. Computers and Fluids 23 (7), 881–893.

Chen, C.H., Liu, H., Beardsley, R.C., 2003. An unstructured, finite-volume, three-dimensional, primitive equation ocean model: application to coastal ocean and estuaries. Journal of Atmospheric and Oceanic Technology 20, 159–186.

Chu, P.C., Fan, C., 1997. Sixth-order difference scheme for sigma coordinate ocean models. Journal of Physical Oceanography 27, 2064–2071.

Davies, A.M., Jones, J.E., 1990. On the numerical solution of the turbulence energy equations for wave and tidal flows. International Journal for Numerical Methods in Fluids 11, 1–25.

Eca, L., 1996. Orthogonal grid generation with boundary point distribution control. Journal of Computational Physics 125, 440.

Edinger, J.E., Brady, D.K., Greyer, J.C., 1974. Heat exchange and transport in the environment. Rep. No. 14, Cooling Water Research Project (RP-49). Electrical Power Research Institute, Palo Alto, CA.

Falconer, R.A., Chen, Y., 1991. An improved representation of flooding and drying and wind stress effects in two-dimensional tidal numerical model. Proceedings of the Institution of Civil Engineers Part 2 91, 659–678.

Fletcher, C.A.J., 1988. Computational Techniques for Fluid Dynamics, vol. 1, Fundamentals and General Techniques. Springer, New York, NY.

Friedrichs, C.T., Aubrey, D.G., 1988. Non-linear tidal distortion in shallow well-mixed estuaries: a synthesis. Estuarine, Coastal and Shelf Science 27, 521–545.

Gordon, R.B., Spaulding, M.L., 1987. Numerical simulations of the tidal- and wind-driven circulation in Narragansett Bay. Estuarine, Coastal and Shelf Science 24, 611–628.

Haidvogel, D.B., Beckmann, A., 2000. Numerical Ocean Circulation Modeling. Imperial College Press, London.

Haight, F.J., 1936. Currents in Narragansett Bay, Buzzards Bay, and Nantucket and Vineyard Sounds. United States Government Printing Office, Washington.

Hamrick, J.M., 1995. Theoretical and computational basis of Environmental Fluid Dynamics Code (EFDC). Special Report No. 17 in Applied Marine Science and Ocean Engineering. Virgina Institute of Marine Science, The College of William and Mary, Gloucester Point, VA 23062.

Haney, R.L., 1991. On the pressure gradient force over steep bottom topography in sigma coordinate ocean model. Journal of Physical Oceanography 21, 610–619.

Huang, W., Spaulding, M., 2002. Reducing horizontal diffusion errors in σ-coordinate coastal ocean models with second-order Lagrangian-interpolation finite difference technique. Ocean Engineering 29, 495–512.

Huang, W., Spaulding, M., 1996. Modeling horizontal diffusion with sigma coordinate system. Journal of Hydraulic Engineering 122 (6), 349–352.

Ip, J.T.C., Lynch, D.R., Friedrichs, C.T., 1998. Simulation of estuarine flooding and dewatering with application to Great Bay, New Hampshire. Estuarine, Coastal and Shelf Science 47, 119–141.

Kantha, L.H., Clayson, C.A., 2000. Numerical Models of Ocean and Oceanic Processes. Academic Press, San Diego, CA, 940pp.

Kinnmark, I., 1985. The Shallow Water Equations; Formulation, Analysis and Application. Springer, New York.

Lin, B., Chandler-Wilde, S.N., 1996. A depth-integrated 2D coastal and estuarine model with conformal boundary-fitted mesh generation. International Journal for Numerical Methods in Fluids 23, 819–846.

Luo, Y., Guan, C., Wu, D., 2002. An eta-coordinate version of the Princeton Ocean Model. Journal of Oceanography 58, 589–597.

Lynch, D.R., Gray, W.G., 1979. A wave equation model for finite element tidal computations. Computers in Fluids 7, 207–228.

Lynch, D.R., Gray, W.G., 1978. Analytical solutions for computer flow model testing. Journal of Hydraulic Engineering ASCE 104 (6), 1409–1428.

Madala, R.V., Piacsek, SA., 1977. A semi-implicit numerical model for baroclinic oceans. Journal of Computational Physics 23, 167–178.

Mellor, G.L., Yamada, T., 1974. A hierarchy of turbulence closure models for planetary boundary layers. Reviews of Geophysics and Space Physics 20 (4), 851–875.

Mellor, G.L., Ezer, T., Oey, L.-Y., 1994. The pressure gradient conundrum of sigma coordinate ocean models. Journal of Atmospheric and Oceanic Technology 11, 1126–1134.

Mellor, G.L., Oey, L.-Y., Ezer, T., 1998. Sigma coordinate pressure gradient errors and the seamount problem. Journal of Atmospheric and Oceanic Technology 15, 1122–1131.

Mesinger, F., 1984. A blocking technique for representation of mountains in atmospheric models. Rivista di Meteorologia Aeronautica 44, 195–202.

Muin, M., Spaulding, M., 1996. Two-dimensional boundary-fitted circulation model in spherical coordinates. Journal of Hydraulics Division, ASCE 122 (9), 512–521.

Muin, M., Spaulding, M., 1997a. Three-dimensional boundary-fitted circulation model. Journal of Hydraulics Division, ASCE 123 (1), 2–12.

Muin, M., Spaulding, M., 1997b. Application of the three-dimensional boundary-fitted circulation model to Providence River. Journal of Hydraulic Engineering 123, 13–20.

Munk, W.H., Anderson, E.R., 1948. Notes on a theory of the thermocline. Journal of Marine Research 1, 276–295.

NGDC, 1996. National Ocean Service, Hydrographic Survey Data, Geophysical Data System (GEODAS) for Hydrographic survey data. National Geophysical Data Center, National Oceanic and Atmospheric Administration, Boulder, CO.

Oey, L.-Y., Mellor, G.L., Hires, R.I., 1985. A three-dimensional simulation of the Hudson-Raritan estuary. Part I: Description of the model and model simulation. Journal of Physical Oceanography 15, 1676–1692.

Officer, C.B., 1976. Physical Oceanography of Estuaries. Wiley, New York, NY, p. 120.

Rady, M.A., El-Sabah, M.I., Murty, T.S., Backhaus, J.O., 1998. Residual circulation in Gulf of Suez. Estuarine, Coastal, and Shelf Science 46, 205–220.

Ries, K. G., 1990. Estimating the surface-water runoff to Narragansett Bay, Rhode Island and Massachusetts. US Geological Survey Water Resources Investigation Report 89-4164, Providence, RI.

Sankaranarayanan, S., Spaulding, M.L., 2003a. A study of the effects of grid non-orthogonality on the solution of shallow water equations in boundary-fitted coordinate systems. Journal of Computational Physics 184 (1), 299–320.

Sankaranarayanan, S., Spaulding, M.L., 2003b. Dispersion and stability analyses of the linearized two-dimensional shallow water equations in boundary-fitted coordinate system. International Journal for Numerical Methods in Fluids 42, 741–763.

Shapiro, R., 1970. Smoothing, filtering and boundary effects. Reviews of Geophysics and Space Physics 8, 359–387.

Shchepetkin, A.F., McWilliams, J.C., 2003. A method for computing horizontal pressure-gradient force in an oceanic model with nonaligned vertical coordinate. Journal of Geophysical Research 108 (C3), 3090.

Sheng, Y.P., 1986. A three-dimensional model of coastal, estuarine and lake currents, using boundary-fitted grid. Technical Report No. 585. Aeronautical Research Associates of Princeton, Princeton, NJ, 1983, p.41.

Signell, R., Geyer, R.W., 1991. Measurements and modeling of the spatial structure of nonlinear tidal flow around a headland. In: Parker, B. (Ed.), Tidal Hydrodynamics. Wiley, New York, 883pp.

Slordal, L.H., 1997. The pressure gradient force in sigma coordinate ocean model. International Journal for Numerical Methods in Fluids 24, 987–1017.

Smolarkiewicz, P.K., Grobowski, W.W., 1990. The multidimensional positive definite advection transport algorithm: non oscillatory option. Journal of Computational Physics 86, 355–375.

Smolarkiewicz, P.K., 1984. A fully multi-dimensional positive definite advection transport algorithm with small implicit diffusion. Journal of Computational Physics 54, 325–362.

Sommerfield, A., 1979. Partial Differential Equations: Lectures on Theoretical Physics, Vol. 6. Academic Press, San Diego, CA.

Song, Y., Haidvogel, D., 1994. A semi-implicit ocean circulation model using a generalized topography-following co-ordinate system. Journal of Computational Physics 115, 228–244.

Spaulding, M.L., 1984. A vertically Averaged circulation model using boundary-fitted coordinates. Journal of Physical Oceanography 14, 973–982.

Stelling, G.S., Duinmeijer, S.P.A., 2003. A staggered conservative scheme for every Froude number in rapidly varied flows. International Journal for Numerical Methods in Fluids 43, 1329–1354.

Stelling, G.S., van Kester, J.A.Th.M., 1994. On the approximation of horizontal gradients in sigma coordinate system. International Journal for Numerical Methods in Fluids 18, 19–35.

Swanson, J.C., 1986. A three-dimensional numerical model system of coastal circulation and water quality. Ph.D. Dissertation. University of Rhode Island, Kingston, RI.

Thompson, J.F., Warsi, Z.U.A., Mastin, C.W., 1985. Numerical grid generation. North-Holland, New York, 1987.

UNESCO, 1981. Tenth report of the joint panel on oceanographic tables and standards. UNESCO Technical Papers in Marine Science No. 36. UNESCO, Paris, 25pp.

Walters, R.A., 2005. Coastal Ocean Models: two useful finite element methods. Continental Shelf Research 25, 775–793.

Wanstarth, J.J., 1977. Nearshore numerical storm surge and tidal model, T. R. H-77-17. US. Army Engineers Wateways Experiment Station, Vicksburg, MS, p. 51.

Ward, M.C., Spaulding, M. L., 2001. A nowcast/forecast system of circulation dynamics for Narragansett Bay. Estuarine and Coastal Modeling, Proceedings of the Seventh International Conference, pp. 1002–1022.

Ward, M.C., 1999. An unsteady finite volume circulation model. Proceedings of the Sixth International Conference on Estuarine and Coastal Modeling, pp. 17–33.

Weisberg, R.H., Sturges, W., 1976. Velocity observations in West Passage of Narragansett Bay: a partially mixed estuary. Journal of Physical oceanography 6, 345–354.

Willemse, J.B.TM., Stelling, G. S., Verboom, G. K., 1985. Solving shallow water equations with an orthogonal coordinate transformation. International Symposium on Computational Fluid Dynamics Delft Hydr. Communication No. 356, January 86, Delft Hydraulics Laboratory, Delft, The Neatherlands.

Xing, J., Davies, A.M., 1996. Application of turbulence energy models to the computation of tidal currents and mixing intensities in shelf edge regions. Journal of Physical Oceanography 26 (4), 417–447.

Zhang, Y.-L., Baptista, A.M., Myers, E.P., 2004. A cross-scale model for 3D baroclinic circulation in estuary-plume-shelf systems: I. Formulation and skill assessment. Continental Shelf Research 24, 2187–2214.